energies

MDPI

Article

Studies on Energy Consumption of Electric Light Commercial Vehicle Powered by In-Wheel Drive Modules

Piotr Szewczyk [1,*] and Andrzej Łebkowski [2]

[1] WB GROUP, Zakład Automatyki i Urządzeń Pomiarowych AREX Sp. z o.o., Hutnicza St. 3, 81-212 Gdynia, Poland
[2] Department of Ship Automation, Gdynia Maritime University, Morska St. 83, 81-225 Gdynia, Poland; a.lebkowski@we.umg.edu.pl
* Correspondence: piotr.szewczyk@arex.pl

Abstract: This article presents the results of energy consumption research for an electric light commercial vehicle (eLCV) powered by a centrally located motor (4 × 2 drive system) or motors placed in the vehicle's wheels (4 × 4 drive system). For the considered constructions of electric drive systems, mathematical models of 4 × 2 and 4 × 4 drive systems were developed in the Modelica simulation environment, based on real data. Additionally, the influence of changes in the vehicle loading condition on the operation of the motor mounted in the wheel and the energy consumption of the drive module was investigated. On the basis of the conducted research, a comparative analysis of energy consumption by electric drive systems in 4 × 2 and 4 × 4 configurations was carried out for selected test cycles. The tests carried out with the Worldwide harmonized Light vehicles Test Cycles (WLTC) test cycle showed a roughly 6% lower energy consumption by the 4 × 4 drive system compared to the 4 × 2 configuration.

Keywords: in-wheel motor; wheel hub motor; electric drive; electric vehicle; battery electric vehicle

Citation: Szewczyk, P.; Łebkowski, A. Studies on Energy Consumption of Electric Light Commercial Vehicle Powered by In-Wheel Drive Modules. *Energies* **2021**, *14*, 7524. https://doi.org/10.3390/en14227524

Academic Editor: Andrea Bonfiglio

Received: 19 September 2021
Accepted: 3 November 2021
Published: 11 November 2021

1. Introduction

The operational properties of electric drive systems, such as no noise emissions or exhaust gases at the place of vehicle operation, high dynamics and high torque generated by the motor in the full rev range, low operating costs, simplicity of design, and small number of mechanical elements, mean that they have become a permanent technology applied by car manufacturers. The positive synergistic effects of the use of an electric driveline can be even better when electric machines mounted in the vehicle's wheels are used for the drive. Directly mounting the motor in a wheel [1,2] increases the efficiency of the vehicle by eliminating elements that generate losses during the transmission of torque, such as gearboxes, mechanical transmissions, differentials, transmission shafts, and drive shafts. On the one hand, the elimination of these elements has a positive effect on the reduction of the vehicle weight, contributing to the reduction of vehicle production costs and environmental protection. On the other hand, the design of the motor increases the unsprung weight of the vehicle and the costs associated with the use of power-electronic converters to control the operation motors [3]. The use of direct drives influences the traction properties of vehicles with motors installed in their wheels [4–6], including the comfort of traveling. This phenomenon may be unfavorable in sports vehicles, where weight minimization due to the occurring overloads is sought. The transmission of vibrations to passengers is related to the height of unevenness on the road, as well as the stiffness and damping of vibrations by the vehicle's suspension. Vibrations with frequencies up to 12 Hz affect all human organs, while vibrations above 12 Hz have a local effect [7]. The low frequencies (4–6 Hz) generated by the cyclic movements caused by the tires rolling on uneven roads can cause resonance phenomena. Prolonged exposure to such

vibrations will aggravate muscle fatigue and make passengers more susceptible to back injury.

Despite the unfavorable increase of the unsprung mass of the vehicle, the ability to steer each wheel in various road situations [8,9], as well as the use of electric regenerative braking [10], provide an opportunity to improve the traction properties of the vehicle [11–13]. At the same time, the use of a direct drive in the wheel requires the implementation of new technological solutions, such as active suspension [14,15] or a spring system for the electric drive module [16–18], the development of various braking algorithms and systems such as anti-lock braking system (ABS), brake assist (BAS), electronic brakeforce distribution (EBD), electronic stability control (ESP) or acceleration slip regulation (ASR), and the use of an electronic differential with the possibility of driving the wheels in the 4 × 2, 4 × 4 system [19]. Motors mounted in the wheels also allow a significant extension of the steering range, giving the vehicle new possibilities in terms of maneuverability. The configuration of the drive system marked with the 4 × 2 symbol most often means that two of the four wheels of the vehicle are driven; similarly, the 4 × 4 configuration means that all four wheels are driven.

Despite the aforementioned advantages, unfortunately, the presence of electric machines in the wheels of vehicles has obvious disadvantages, mainly related to energy storage, i.e., the high cost of the battery cells and the low energy density translating into the short range of the vehicle. At the same time, these types of drive systems are able to meet the stringent regulations related to the limitation of exhaust emissions by vehicles, as well as the procedures related to their measurement [20]. These regulations have been implemented in order to address the issues of climate change, deterioration of air quality, and increased mortality among people caused by the impact of transport [21–24]. As a result of the proposed restrictions, it is planned to completely eliminate vehicles with combustion engines in some countries from 2025 (Norway), in others from 2030 (Denmark, the Nederlands, Ireland, Slovenia, Sweden, Israel), 2035 (Great Britain), 2040 (France, Spain, Egypt, China (Hainan)) and 2050 (Germany, Canada, USA) [25].

Along with the development of electric drive technology in the automotive industry, in recent years, category N1 electric light commercial vehicles (eLCV) have appeared [26], the most popular of which are the Citroen Relay Electric, Fiat Ducato Electric, Ford e-Transit, Mercedes eSprinter, Nissan e-NV200, Peugeot e-Boxer, Renault Master ZE, Vauxhall Vivaro-e, Volkswagen e-Crafter, LEVC VN5, Maxus EV80 and others [27,28]. Most of the available vehicles, with a permissible total weight of 3500 kg, an energy storage capacity of 40 to 80 kWh and a payload of 900 to 1300 kg, offer a range of 170 to over 350 km. Virtually every electric drive system in the aforementioned vehicles consists of an energy storage module located under the floor of the vehicle with power electronics ensuring its charging, and an inverter controlling the operation of a centrally mounted electric motor, which drives the wheels of the vehicle through a transmission or gearbox (Figure 1a).

In some eLCV solutions, a hybrid system in the form of an internal combustion generator is used to increase the range [29]. Another solution (Figure 1b–d) to this limitation is to place the drive motors with inverters in the immediate vicinity of the vehicle wheels and drive them through a transmission or directly via a drive shaft [30]. There are also solutions where electricity is transmitted wirelessly to the motor located in the wheel or its immediate vicinity [31,32].

Among the designs of electric drive systems, those with electric motors located directly in the wheel are evolving rapidly. The vast majority of these designs use synchronous motors with permanent magnets, such as outrunner radial flux [33–40], axial flux [41–48], reluctance [49,50] or induction [51,52]. There are also constructions that, in order to reduce exhaust emissions generated by heat engines, use drive modules that can be added to an existing internal combustion vehicle by replacing parts of the suspension components [53,54] or the entire axle [55].

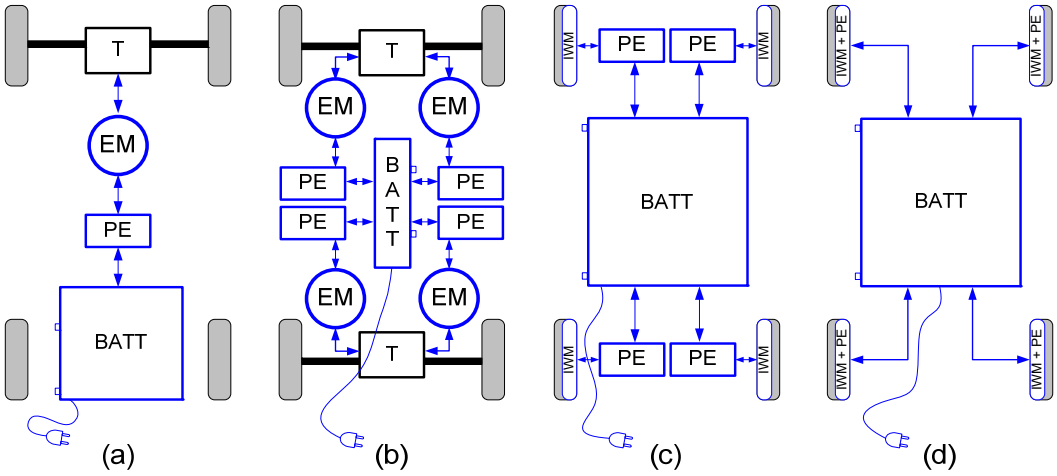

Figure 1. Examples of configurations of the electric drive systems of delivery vehicles (**a**) central driveline with one electric motor, (**b**) power train with four electric motors installed on board the vehicle, (**c**) a driveline with four electric motors installed in the wheels of the vehicle and inverters on board the vehicle, (**d**) drive system with four electric motors and inverters installed in the wheels of the vehicle, where: BATT—Battery Pack; PE—Power Electronics (Inverter); EM—Electric Motor, T—transmission.

This publication presents the results of research on an electric drive module, consisting of a wet brake integrated within an electric motor and mounted in a vehicle wheel. The wet brake contributes to the reduction of dust emissions, a phenomenon associated with normal braking systems due to the brake pads and discs rubbing against each other. The present research covers the impact of changes in vehicle weight, as well as changes in the weight of the drive system components, on the strength of the suspension components, as well as the changing rolling resistance. For the considered electric drive unit design, mathematical models of 4 × 2 and 4 × 4 drive systems were developed in the Modelica simulation environment (modelica.org) on the basis of real research. The 4 × 2 driveline uses one motor, centrally transmitting drive torque via the gears/axle to the rear wheels of the vehicle. The 4 × 4 system uses four independent motors installed in the vehicle's hubs, transmitting the drive torque directly to the vehicle wheels. On the basis of the conducted research, a comparative analysis of energy consumption by electric drive systems in 4 × 2 and 4 × 4 configurations was carried out for selected test cycles.

2. Models and Methods

The development of an accurate model of a delivery vehicle with electric drive, which includes many cooperating elements, is a complex task which requires some experience. This chapter presents the models and simulation tools that were used to determine the electricity consumption of an electric light commercial vehicle (eLCV). Two types of drive systems were analyzed: a central one with one electric motor (4 × 2) transmitting torque via a transmission to the rear wheels of the vehicle (Figure 1a), and another with motors built into the wheels (4 × 4), transmitting torque directly to the vehicle wheels (Figure 1c). To estimate the forces occurring in the electric drive unit intended for the eLCV type vehicle, a test stand was developed on which the tests were carried out. The obtained results were used to develop a mathematical model. The data on the basis of which the mathematical models of vehicles in 4 × 2 and 4 × 4 configurations were developed come from measurements recorded on real vehicles.

2.1. Mathematical Model of an eLCV Type Vehicle

The structure of the delivery vehicle is influenced by fundamental forces shown in Figure 2. They are related to the resistance to motion caused by the following parameters: the force of gravity F_{GR}; the force of the vehicle pressing on the ground F_N; the sliding force F_S; forces related to the aerodynamic drag of the vehicle F_A, which mainly depend on

the shape and geometrical dimensions of the vehicle; forces related to rolling resistance F_R, depending on the surface on which the vehicle moves and the parameters of the tire; and Forces related to resistances in the torque transmission F_D. Moreover, when the vehicle is moving, it is subjected to additional forces resulting from unevenness in the road, the operation of the suspension system, the operation of the motor depending on the technology used, as well as the transmission of the drive torque between the drive motor and the surface on which the vehicle is moving. In order for the vehicle to move, a force counteracting the forces mentioned above must be generated by the vehicle drive system, i.e., the driving force F_M.

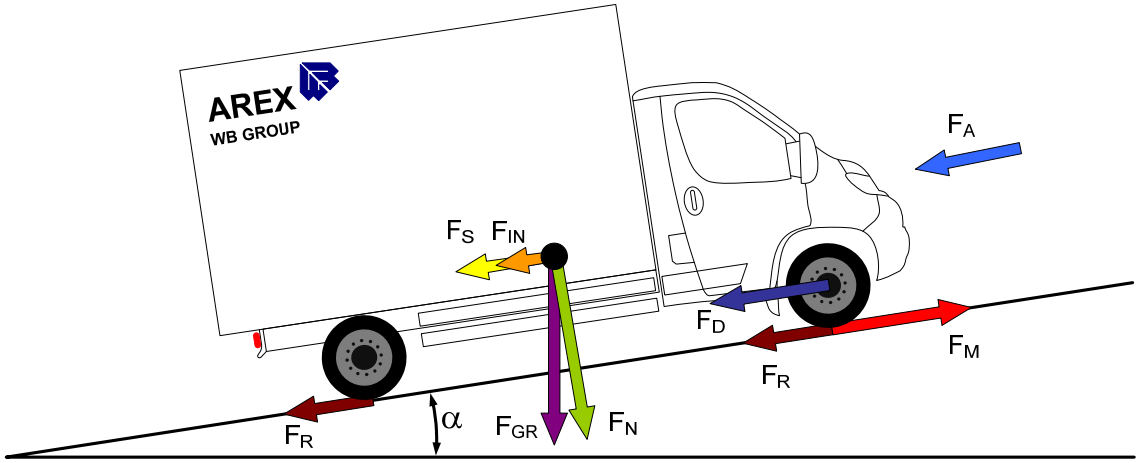

Figure 2. Forces acting on a moving eLCV.

The sum of the forces acting on the body of the delivery vehicle can be described by the following equation:

$$F_M = F_A + F_R + F_S + F_{IN} + F_D \quad (1)$$

where F_A is the total aerodynamic drag force, F_R is the total resistance of the vehicle, F_S is the total sliding force, F_{IN} is the total inertia force of the vehicle, and F_D is the total resistance related to the transmission of torque in the drive system.

The aerodynamic resistance can be determined from the relationship:

$$F_A = C_d \cdot A \cdot \frac{\rho \cdot v^2}{2} \quad (2)$$

where C_d is the coefficient of aerodynamic drag of the vehicle [-]; A is the frontal area of the vehicle [m^2]; v is the vehicle velocity [m/s]; and ρ is the ambient air density [kg/m^3].

A very important element influencing the value of the force associated with aerodynamic resistances is the C_d coefficient. The smaller its value, the lower the aerodynamic resistance of the vehicle, which translates into an increase in range. For example, the C_d value for mass-produced passenger cars ranges from 0.19 to 0.4, and for vans and trucks from 0.35 to 0.9 [56,57].

The rolling resistance of a vehicle can be determined on the basis of the relationship:

$$F_R = m \cdot g \cdot \mu \cdot \cos(\alpha) = m \cdot g \cdot \frac{\mu_R}{r} \cdot \cos(\alpha) \quad (3)$$

where m is the vehicle weight [kg]; g is the standard gravity [m/s^2]; μ is the dimensionless rolling resistance coefficient of the vehicle [-]; μ_R is the rolling resistance coefficient of the vehicle [m]; r is the vehicle wheel radius [m]; α is the road inclination [deg]; and a is the acceleration of the vehicle [m/s^2].

The rolling resistance coefficient for a pneumatic tire running on a dry road can be estimated from the relationship [58]:

$$\mu = 0.005 + \left(\frac{1}{p}\right) \cdot \left(0.01 + 0.0095 \cdot \left(\frac{v}{100}\right)^2\right) \tag{4}$$

where μ is the dimensionless rolling resistance coefficient of the vehicle [-]; p is the tire pressure [bar]; and v is the vehicle velocity [km/h].

The vehicle sliding force was determined on the basis of the dependence:

$$F_S = m \cdot g \cdot \sin(\alpha) \tag{5}$$

The resistances related to the inertia forces caused by acceleration and braking were calculated on the basis of:

$$F_{IN} = m \cdot a \tag{6}$$

The vehicle structure is also affected by the forces associated with the transmission of torque to the wheels and the related losses:

$$F_D = \frac{T_{DS} \cdot \omega_{DS}}{\omega_{nDS} \cdot r} \tag{7}$$

where T_{DS} is the torque at the drive shafts at the rated speed [Nm]; ω_{DS} is the average speed of wheel drive shafts [rad/s]; and ω_{nDS} is the nominal rotational speed of the wheel drive shafts [rad/s].

The driving torque generated by the electric motor is the source of the driving force F_M transmitted by the differential and the driveshafts to the vehicle wheels (4 × 2), or directly by the motor located in the wheel (4 × 4).

$$F_M = \frac{T_M \cdot k_D}{r} \tag{8}$$

where T_M is the torque produced by the electric motor [Nm]; and k_D is the differential gear ratio [-].

The efficiency of the electric drive system with a differential (4 × 2) can be determined on the basis of the relationship:

$$\eta_{4\times2} = \eta_B \cdot \eta_I \cdot \eta_M \cdot \eta_D \tag{9}$$

where η_B is battery efficiency (energy storage) [-]; η_I is inverter efficiency [-]; η_M is motor efficiency [-]; and η_D is the efficiency of the differential [-].

The efficiency of an electric drive system with motors located in the wheels (4 × 4) can be determined on the basis of the relationship:

$$\eta_{4\times4} = \frac{P_{OUT1} + P_{OUT2} + P_{OUT3} + P_{OUT4}}{\frac{P_{OUT1}}{\eta_{M1}} + \frac{P_{OUT2}}{\eta_{M2}} + \frac{P_{OUT3}}{\eta_{M3}} + \frac{P_{OUT4}}{\eta_{M4}}} \tag{10}$$

where $\eta_{M1}, \eta_{M2}, \eta_{M3}, \eta_{M4}$ are the efficiencies of electric drive modules M1, M2, M3, M4, respectively [-]; and $P_{OUT1}, P_{OUT2}, P_{OUT3}, P_{OUT4}$ describe the effective power of electric drive modules M1, M2, M3, M4, respectively [kW].

The movement of the vehicle on the road is associated with the occurrence of various types of resistance. The moving wheel of a loaded vehicle is a source of resistance, which may be broken down as follows: aerodynamic resistance constituting approx. 1.5–3.5% of the total wheel resistance, rolling resistance between the tread and the ground (friction at the contact of materials, roughness of rolling surfaces) amounting to approx. 2–10% and the resistance related to the transmission of torque to the wheels of the vehicle, deflection

of the side edges (elastic properties of materials) and the work of the tires themselves, i.e., 90–95%.

The total take-off share associated with forces acting on the vehicle structure is also associated with elements such as:

- the type of tire and the material from which it is made;
- tire pressure (higher pressure → lower rolling resistance → worse grip);
- the vehicle loading condition (heavier vehicle → higher rolling resistance);
- wheel alignment setting (incorrect wheel alignment → higher rolling resistance);
- tire tread depth (smaller tread → lower rolling resistance → worse grip);
- vehicle speed (speed increase → greater rolling resistance);
- road surface (concrete (μ = 0.01), asphalt (0.02), compacted crushed stone (0.02), small paving stones (0.015), pavement (0.03), solid sand (0.04), loose gravel (0.06), medium hard soil (0.08), hard soil (0.1–0.15), sand, mud (0.2–0.35);
- occurrence of torque (occurrence of accelerating or braking torque → lower rolling resistance) [59].

The development of a mathematical model that takes into account the effects of basic and additional forces on the vehicle structure is a complicated task.

For this reason, a mathematical model of a light delivery vehicle with an electric drive was implemented in the Modelica environment. This model was designed for two electric drive system configurations. The first uses a DCE-200 (Drive CEntral) midmotor driveline (η_M = 0.94%) which transfers torque through differentials (η_D = 0.92%) to the vehicle axles. This system is abbreviated as 4 × 2. The central motor is driven by the STS-202 inverter (η_I = 0.98%), drawing energy from the BAT-200 energy storage (η_B = 0.94%). In the second configuration, the single motor and reduction gear are replaced with four smaller DWH-200 motors (Drive WHeel) (η_M = 0.92%) that directly drive all four wheels. This system is abbreviated as 4 × 4. DWH-200 motors located in the wheel arches of the vehicle are controlled by four STS-203 inverters (η_I = 0.98%), with each inverter independently controlling the operation of each motor. For the developed elements of the real drive system with a differential (4 × 2), the total efficiency of the electric drive system was about 80%. For an electric drive system with motors located in the wheels (4 × 4), the efficiency of the system was approximately 85%.

2.2. Simulation Model of an eLCV Type Vehicle in the Modelica Environment

The structure of the electric drive system of the central motor eLCV modeled in the Modelica environment is presented in Figure 3.

The presented model consists of the following blocks: block modeling the dimensions and related physical properties of the eLCV vehicle, driving axle block, DCE-200 motor block (power up to 300 kW, maximum torque 2400 Nm), STS-202 inverter block (max. power up to 300 kW, DC-link voltage 12-850 VDC), power data analyzing block, BAT-200 energy storage block, route profile setting block, and electric load block for 12 VDC installations.

The challenge of modeling the physical parameters of an eLCV vehicle is to reproduce the physical properties of the test vehicle on which the traction tests were carried out, i.e., the Peugeot Boxer, as faithfully as possible. The following physical phenomena were taken into account in the block representing the properties of the Peugeot Boxer test vehicle: vehicle movement, including the rolling resistance of the wheels on the road; the action of forces on the vehicle body when overcoming terrain slopes; aerodynamic drag and inertia forces. The eLCV model with a central motor also includes a model of drive wheels equipped with tires of the size 195/75/R16, which are driven by the torque coming from the electric motor, transmitted to the wheels via a transmission located in the drive axle. For the purposes of the simulation, it was assumed that the modeled wheels had a radius of 349 mm, and roll without skidding on the surface on which the vehicle was moving. Other parameters used by the eLCV model with central motor included the mass of the vehicle,

the frontal area of the vehicle, the coefficient of aerodynamic drag, and the coefficient of rolling resistance of the vehicle wheels on a given surface.

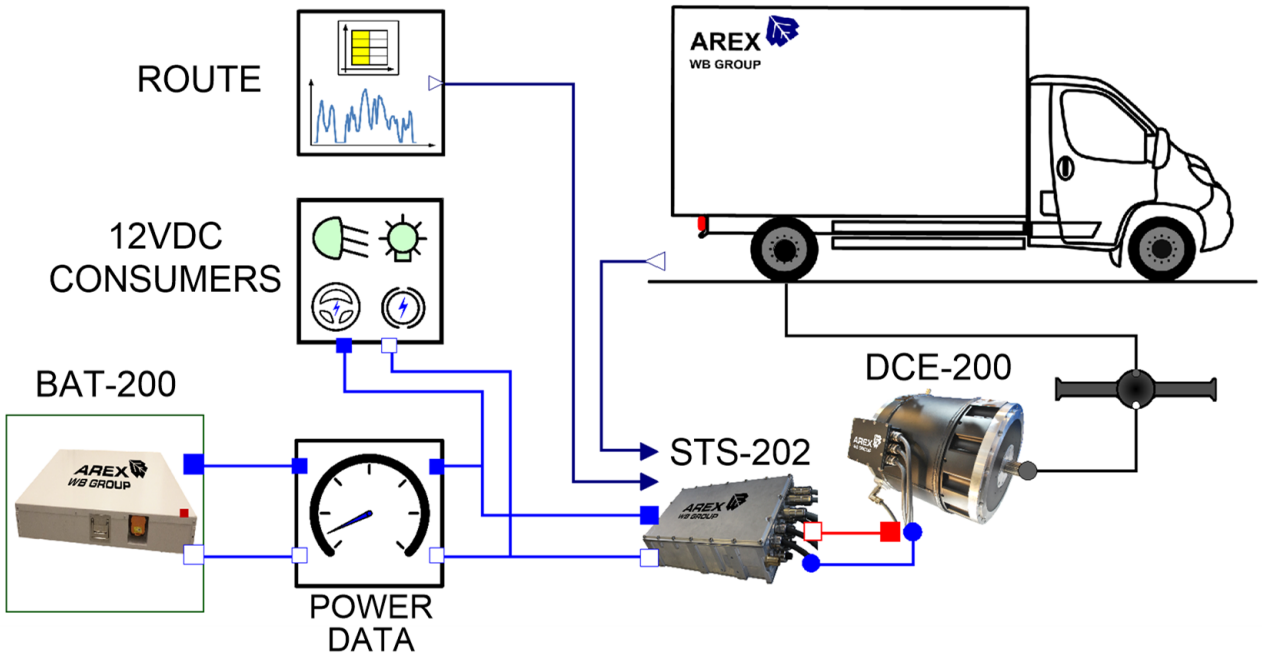

Figure 3. Model structure of eLCV electric powertrain with central motor (4 × 2).

The developed model of the block for specifying the route profile enabled the introduction of test routes with a specific speed profile as a function of time, as well as the vehicle inclination as a function of the distance traveled. For research, it is possible to use test routes with either a constant or variable slope. Synthetic test routes such as the WLTC test family [60] or the previously used the New European Driving Cycle (NEDC) tests [61] predict road driving without any gradients. For the purposes of the research, the actual traffic was recorded and the parameters of the test routes (Gdynia-Flat, Gdynia-Hills) were developed, enabling the determination of the slope profile of the test route and the speed on individual sections. Based on the known parameters of the route, the value of the slope angle was determined and used to calculate the sliding force acting on the vehicle on a given section of the test route. The main task of the route profile block was to provide the set speed signal, which was taken into account in the process of controlling the operation of the traction motor/motors controlled by the inverter/inverters.

The driving axle block contains a model of a reduction gear with a differential where the driving torque generated by the vehicle's central motor is transmitted to the wheels of the rear axle of the vehicle. It was assumed that the reduction gear ratio was 1:3.6. Additionally, the resistances of internal mechanisms that occur during its operation were modeled in the bridge block.

The electric motor block was used to model the behavior of the DCE-200 permanent magnet synchronous motor. The block comprised elements from the standard library of the Modelica package, modeling a synchronous electric machine excited by permanent magnets, and sensors of rotational speed, phase currents and the position of the motor shaft.

The STS-202 inverter block modeled the operation of the inverter powering the synchronous motor. In addition to the inverter actual model, the block also included a vehicle linear speed controller that controlled the torque generated in the DCE-200 motor driven by the inverter. The speed controller was implemented as a PI type controller that used the speed command signal generated in the route profile setting block and the actual speed signal supplied from the light delivery vehicle block. At the output of the speed regulator,

the value of the desired motor current was obtained, the value of which controlled the operation of the inverter. The STS-202 inverter block modeled the transfer and conversion of direct current electric energy, taken from the input terminals, into alternating current energy supplying the synchronous motor. Modeling the process of converting electricity took into account the efficiency of the inverter through an efficiency map.

The energy source of the modeled vehicle was a block containing the BAT-200 energy storage model. It represents an energy storage system based on 198 LiFePO4 electrochemical cells with a capacity of 100 Ah each, connected in series in a 198S1P system. The energy storage model block allowed us to model operation at different cell initial temperatures and different initial charge states. The basic parameter modeled by the energy storage block was the State of Charge (SOC) of the electrochemical cells included in the storage. The process of discharging the energy store lowered the SOC value, while charging increased it. Exceeding the SOC value during the simulation of the range <0; 1> caused the immediate termination of the simulation. The state of charge of the cells had a direct impact on the voltage generated by these cells. The curve of the dependence of the voltage of LiFePO4 cells on their state of charge used in the model is presented in Figure 4. LiFePO4 cells are characterized by a relatively flat course of the voltage curve between SOC in the range <0.1; 0.9>. The block of the energy storage model allowed us to model the operation at any initial state of charge in the range <2.2; 3.6> VDC.

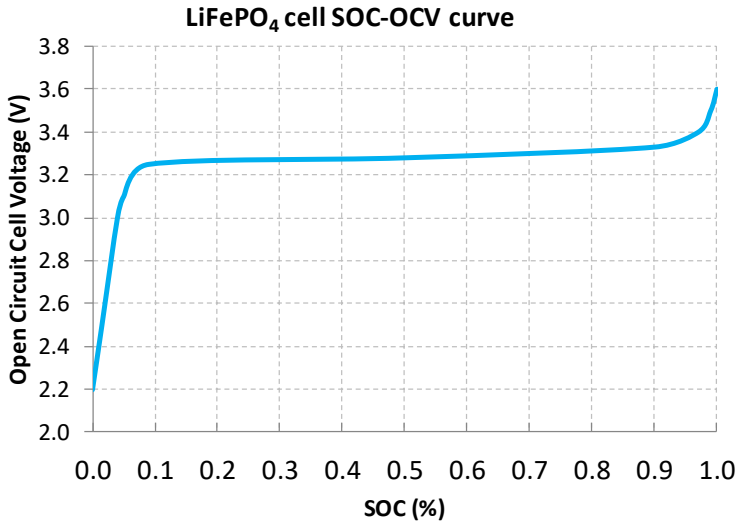

Figure 4. The course of voltage changes of a single LiFePO4 cell, depending on the State of Charge (SOC).

The thermal model of LiFePO4 cells, taking into account the change in the internal resistance of the warehouse depending on the cell temperature, took into account the heating of the cells under the influence of the electric current flowing in the circuit during the discharge and charging of the energy storage. The process of exchanging the thermal energy of the cells with the environment through the housing of the energy storage was also included, as well as the possibility of using the thermal conditioning system of the energy storage to heat the cells, e.g., when the vehicle is parked, at low ambient temperature. Cell cooling causes a greater voltage drop associated with an increase in internal resistance, which, when used in a vehicle, translates into higher current consumption, necessary to maintain the power required by the driver. Increased current flow at low temperature translates into higher consumption of energy storage cells and a lower State of Health (SOH). The block of the energy storage model allowed us to model the operation at different initial temperatures of the cells.

The operation of the energy storage thermal conditioning system was modeled by specifying the power of the heat flux, expressed in watts, delivered in the case of heating, or received in the case of cooling, to the electrochemical cells of the energy storage.

In addition, the energy flow management model took into account elements such as: vehicle operation profile (Normal, Eco, Sport, Safe); operating states of the electric machine (engine work/generator work; power, torque and rotational speed generated by the electric machine); implementation of tasks related to torque vectoring and traction control; and DC-link voltage regulation for energy storage with built-in DC/DC buck-boost converters.

The 12 VDC electrical load block was used to model the energy consumption of the low-voltage part of the vehicle's electrical installation, supplied with energy from the BAT-200 energy storage through the DC/DC voltage converter. The model assumed a constant low voltage load power, which corresponded to the average power consumption of the vehicle's components and systems, such as external and internal vehicle lighting, and electronic devices such as the vehicle's instrument panel, power steering and braking systems. The low-voltage circuit was powered from the PSU-203 DC/DC converter, taking energy from the BAT-200 warehouse. Taking into account the power consumed by the on-board receivers, a constant load power of the BAT-200 energy storage was assumed, equal to 500 W.

The last block of the vehicle model was a tool block whose task was to analyze energy consumption. This block was used to measure, among others things, total energy consumption, energy consumption coefficient per unit of distance traveled, estimated range, power consumed by the drive system and low voltage installation converter. This block used the voltage and electric current sensors that are part of the Modelica standard library.

The structure of the drive system in the configuration with electric motors located in the wheel hubs is shown in Figure 5. The simulation model consisted of the following elements: light delivery vehicle block, DWH-200 motor blocks (maximum power up to 100 kW, maximum torque 1000 Nm), STS-203 inverter blocks (power up to 100 kW, DC-link 12-850 VDC voltage), power data analyzing block, BAT-200 energy storage block, route profile setting block, and block of electric loads for 12V installations.

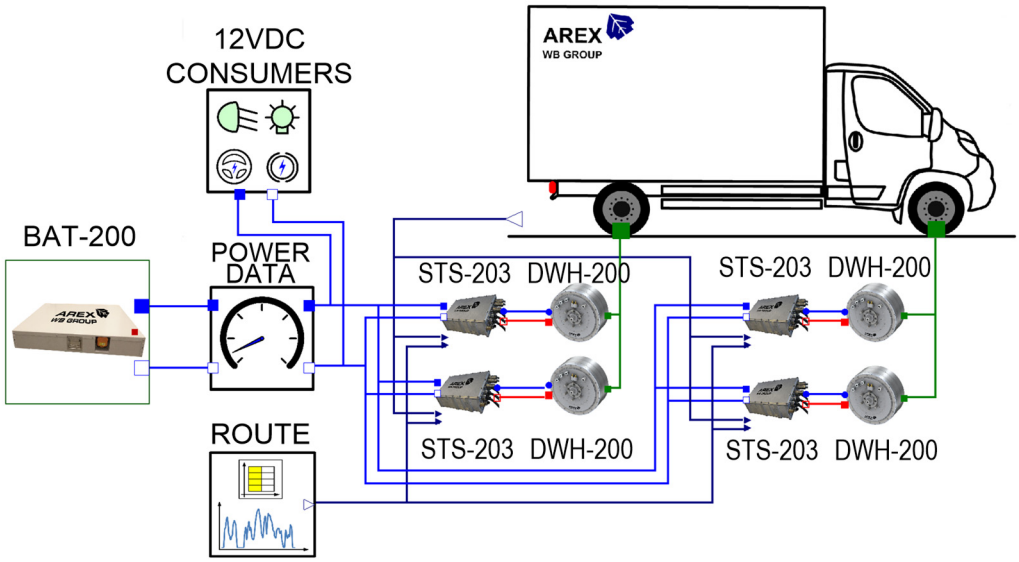

Figure 5. View and structure of the light delivery vehicle model with the drive system using electric motors located in the wheel hubs.

The light commercial vehicle block performed the same functions as in the mid-motor configuration, except that it did not include the drive wheel models that were transferred to the DWH-200 motor blocks.

The DWH-200 motor blocks were used to model the electric motor and wet brake assemblies in one housing, mounted in the hub of a standard 16-inch radius wheel and fitted with a 195/75/R16 tire. The DWH-200 electric motor is also a permanent magnet synchronous motor, and its model used the same configuration of elements from the standard library of the Modelica package as the DCE-200 motor model, of course with appropriately changed parameters depending on the type and properties of the motor in question.

The STS-203 inverter block had the same configuration and functions as the STS-202 inverter block in a configuration with a central motor. An important difference was the other PI speed regulator settings, related to the different characteristics of the DWH-200 motors, their lower rotational speed, and about four times less power compared to the DCE-200 motor. In the modeled system, each of the STS-203 inverters worked independently, but they worked to drive one vehicle, and were therefore connected through the surface on which the vehicle was moving.

The other blocks of the model in the configuration with direct drive wheels performed the same function as in the configuration with the center motor.

2.3. Stand for Testing the Electric Drive Unit

In order to obtain the necessary data to conduct simulation tests of energy consumption by a vehicle with motors placed in the wheels, a physical test stand was developed. This stand was used to estimate the forces occurring in the electric drive unit of the eLCV vehicle. As a result of the research, the values of resistances generated by the electric drive module depending on the load of the vehicle associated with its loading were determined. The factory suspension of the vehicle was also tested in order to determine its strength after installing the electric drive module instead of a classic wheel. An image of the test stand is shown in Figure 6.

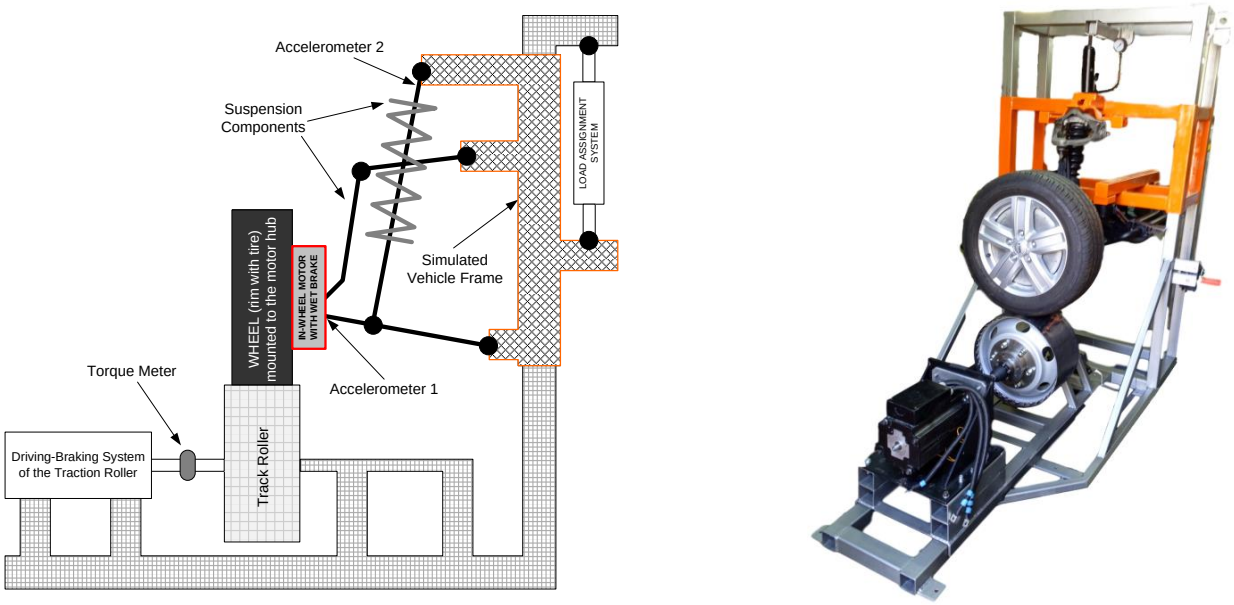

Figure 6. Construction of the stand for testing the electric drive unit and suspension. Right: view of the actual stand.

The developed research stand enabled the implementation of research in the field of:

- setting a variable load, simulating the variable loading of the vehicle in the range of up to 1500 kg per wheel,
- setting the torque (braking/driving) for the working drive module by the traction roller,
- setting the acceleration variable for the drive module caused by the suspension vibrations while moving on different surfaces simulated with the use of four inter-

changeable traction rollers, marked with the symbols: R1-flat surface such as asphalt, concrete; R2-gravel, sand surface; R3-pavement type surface; R4-pavement simulating driving over a beam or driving on a rocky, bumpy road.

In-Wheel Motor DWH-200 with Wet Brake

An electric drive unit consisting of a synchronous DWH-200 motor with a wet brake, placed in the wheel of a van with a maximum permissible weight of 3500 kg, was tested. Figure 7 shows the prototype and a cross-section of the DWH-200 motor with a wet brake.

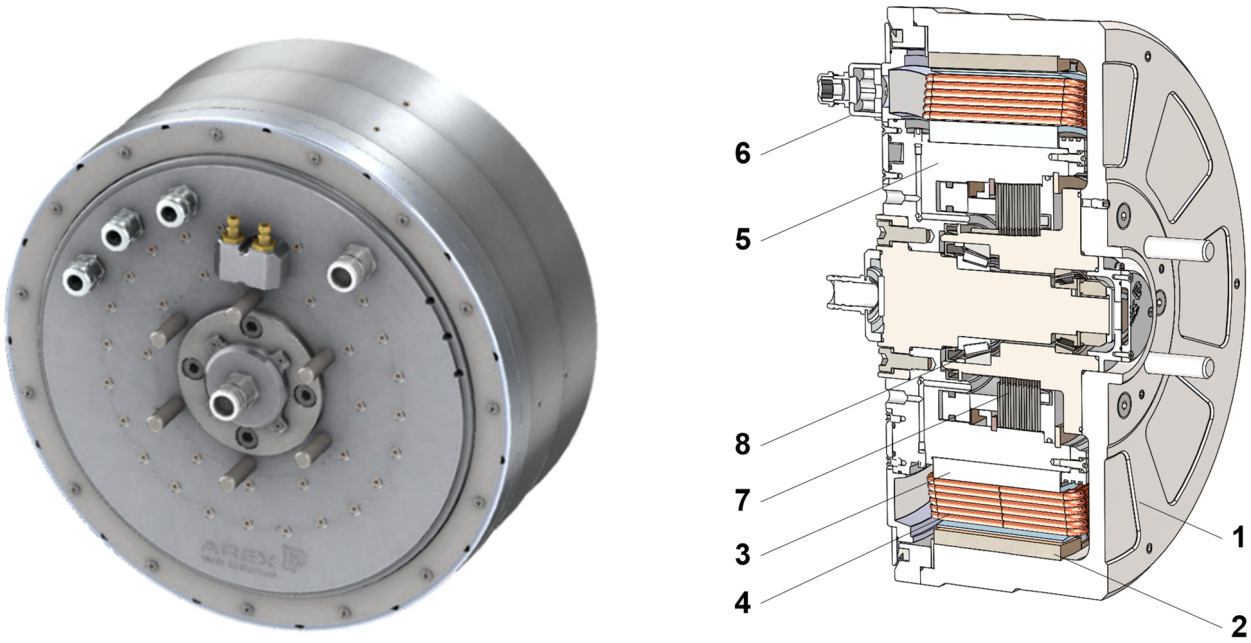

Figure 7. View of the prototype and a cross-section of the drive module for mounting in the Electric Light Commercial Vehicle wheel developed by AREX Sp. z o.o. 1—rotor, 2—magnets, 3—stator's magnetic core, 4—stator winding coils, 5—supporting structure, 6—entry for supply wires, 7—wet brake, 8—bearings system.

Table 1 shows the mass balance of the tested suspension system for one quarter of the vehicle. After performing the relevant calculations, the unsprung mass of the suspension system with the electric drive unit was found to be 150.63 kg, the unsprung mass of the classic drive system was 79.41 kg, the tire size used during the tests was 225/55/R17C, tire load index was 109 (1030 kg) and the rim load index was 1060 kg.

Table 1. Weights of the tested drive module with the DWH-200 motor.

Item Name	Drive Unit Weight (kg)	Classic Wheel Weight (kg)
DWH-200 motor with wet brake	90.00	–
Rim with tire	25.00	25.00
Brake caliper	–	9.43
Brake disc	–	9.35
Clamping screws	0.47	0.47
Steering	12.76	12.76
Shock absorber with spring	14.50	14.50
The upper control arm	2.30	2.30
Lower control arm	5.60	5.60
TOTAL	150.63	79.41

3. Results

In the course of the research, the impact of changes in the vehicle weight and in the weight of the drive system components on the strength of the suspension components, as well as the changing rolling resistance, was verified. The results of this research were used to conduct simulation tests in the Modelica environment. On this basis, two 4 × 2 drive systems with one central motor and 4 × 4 with four motors located in the wheels of the vehicle were analyzed. The conducted research was used to evaluate the energy consumption of electric drive systems in 4 × 2 and 4 × 4 configurations.

3.1. Research of the Electric Drive Unit

The conducted research was aimed at verifying the influence of changes in vehicle weight and drive system components on the strength of suspension components as well as rolling resistance. The tests were carried out for three vehicle suspension load values: 400 kg (Gross Vehicle Weight GVM = 1600 kg), 750 kg (GVW = 3000 kg), and 900 kg (GVW = 3600 kg). The tests were carried out for four simulated road surfaces: R1-flat pavement such as asphalt, concrete; R2-gravel, sand surface; R3-pavement type surface; R4-pavement simulating driving over a beam or driving on a rocky, bumpy road.

The tested integrated drive system module consisted of the DWH-200 electric drive motor, the WHB-200 wet brake motor, the wheel hub as an interface for the assembly of standard wheel rims, the cooling system, suspension elements (steering knuckle, rocker arms, brake caliper with pads, shield and disc, steering rod, spring with shock absorber, stabilizer), which were mounted to the modeled body parts of the vehicle.

The stand tests of the suspension module with a built-in drive system were carried out on the basis of strength and vibration tests, developed according to the ISO16750-3 standard, Test IX—"Commercial vehicles. Unsprung mass".

During the research, the following parameters were recorded:

- DWH-200 motor speed,
- power and torque generated by the DWH-200 motor,
- accelerations in the X, Y, Z axes in the place where the motor is mounted to the vehicle suspension,
- accelerations in the X, Y axes at the place of mounting the suspension to the vehicle frame.

3.1.1. Research on the Influence of Vehicle Load Changes on Vibrations of the Drive Module

In the course of the research, the influence of changes in the vehicle mass on the change of the acceleration amplitude was verified. Figure 8 shows the recorded values of the acceleration amplitude on the Y axis as a function of time for loads of 400 kg, 750 kg and 900 kg with R1, R2, R3 and R4 rollers. The rotational speed of the rollers was changed in the range from 0 to approx. 100 km/h.

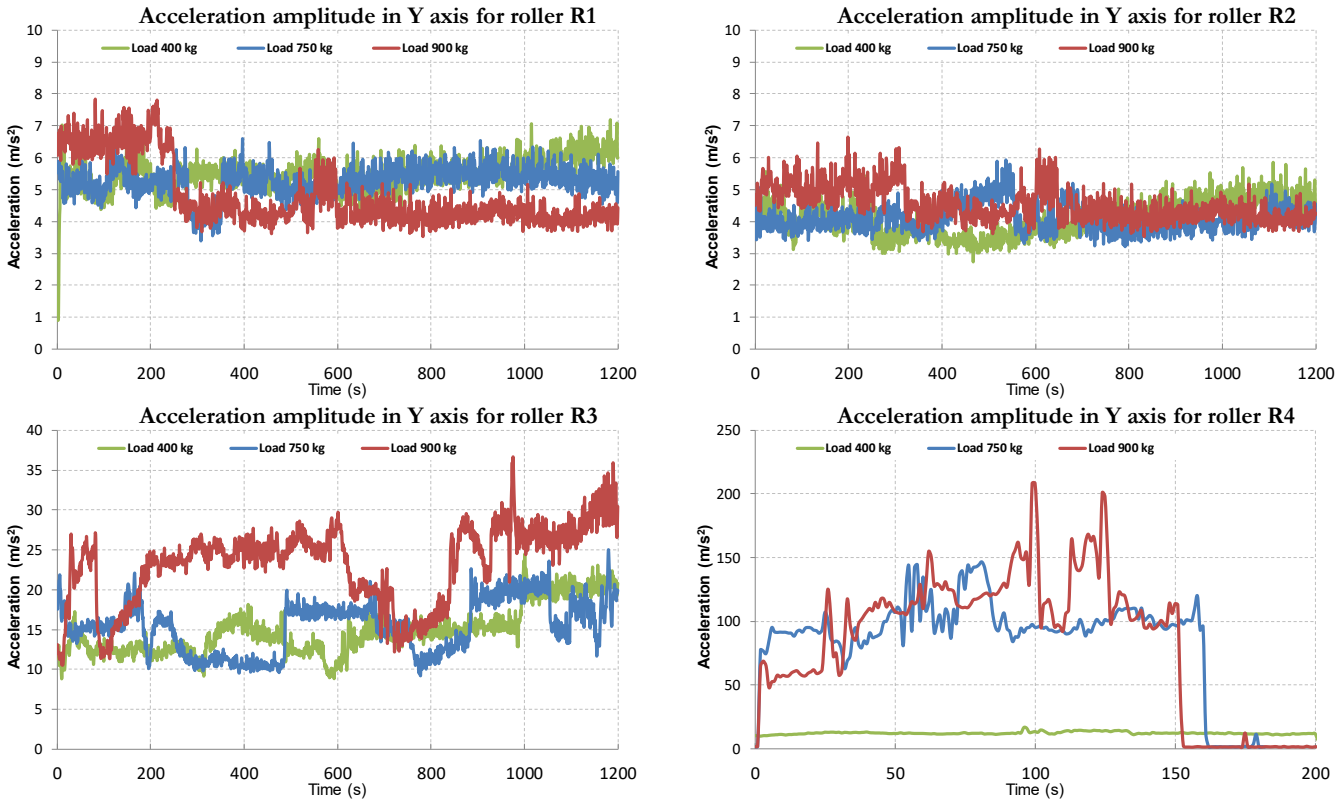

Figure 8. The value of the acceleration amplitude in the Y axis as a function of time, for loads of 400 kg, 750 kg and 900 kg with rollers R1, R2, R3 and R4.

3.1.2. Research on the Influence of Tire Pressure Changes on Vibrations of the Drive Module

In the course of the tests, the influence of changes in tire pressure in the range from 1.0 bar to 5.5 bar on the vibrations of the drive unit was verified. The tests were carried out for two vehicle speeds, i.e., 30 km/h (time range 0–100 s in the figures) and 50 km/h (time range 100–200 s in the drawings), with a fixed load of 750 kg on a flat surface (roll R1). The results of the obtained tests are presented in Figure 9.

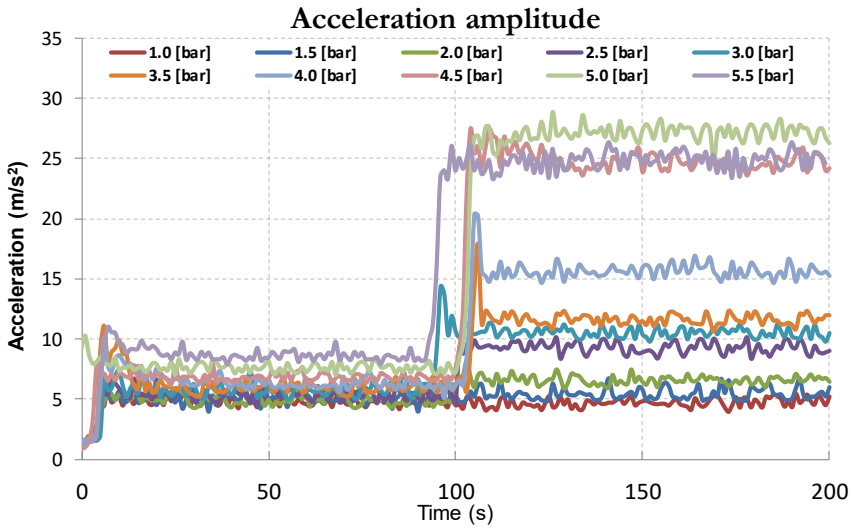

Figure 9. Influence of changes in tire pressure on vibrations of the drive unit.

3.1.3. Research on the Influence of Tire Pressure Changes on Energy Consumption

The influence of changes in tire pressure in the range of 1.0 bar to 5.5 bar on the energy consumption of the electric drive unit was verified. As in Section 3.1.2, the tests were carried out for two vehicle speeds, i.e., 30 km/h and 50 km/h, with a fixed load of 750 kg on a flat surface (roller R1). The results are presented in Figure 10.

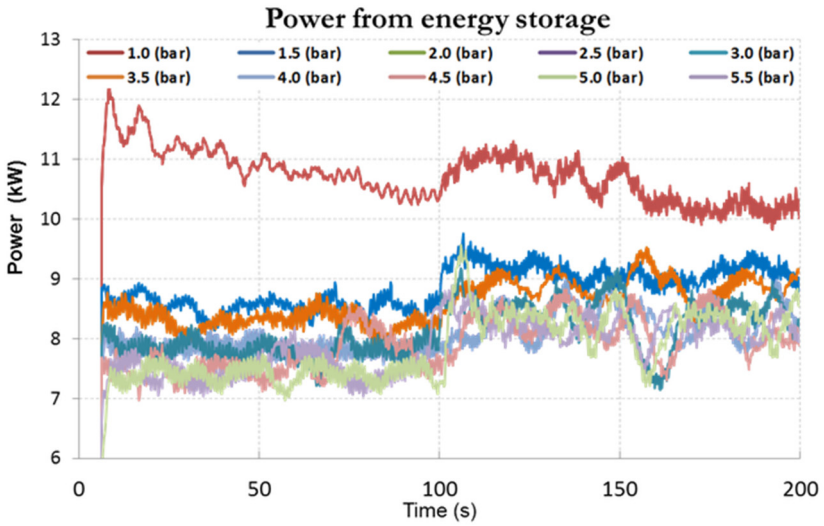

Figure 10. Influence of tire pressure changes on energy consumption from an accumulator package.

3.2. Tests of Energy Consumption by an Electric Drive 4 × 2

The mathematical model of the electric drive vehicle in the 4 × 2 configuration, presented in Section 2.1, was used for the tests. The electric drive system included one DCE-200 electric motor, capable of developing a maximum power of 300 kW and a torque of 2400 Nm. The motor was powered by the STS-202 inverter, which enabled the control of drives up to 300 kW, with a supply voltage from 12 to 850 VDC. The research was carried out on the basis of the WLTC test cycles [61] (Figure 11) and the Gdynia-Flat test cycle (Figure 12), which was developed internally. The main purpose of this research was to estimate the energy consumption of the drive system in a 4 × 2 configuration. The results of the conducted research are presented in Figures 13–15.

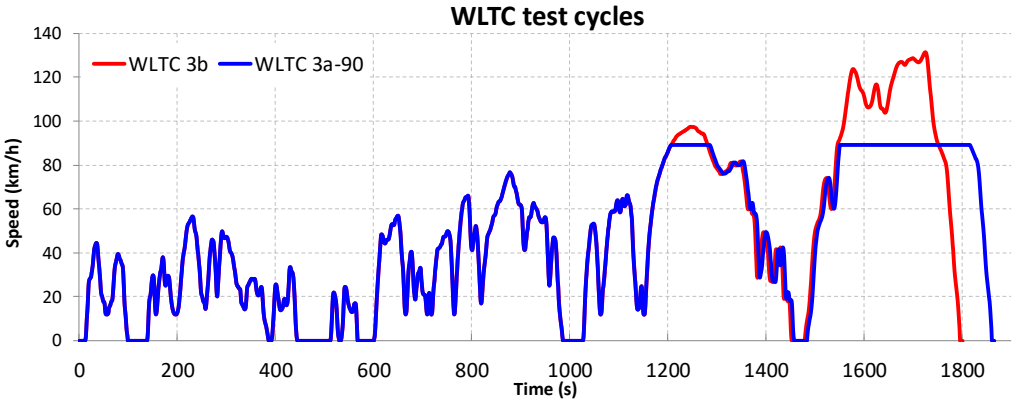

Figure 11. WLTC driving cycles.

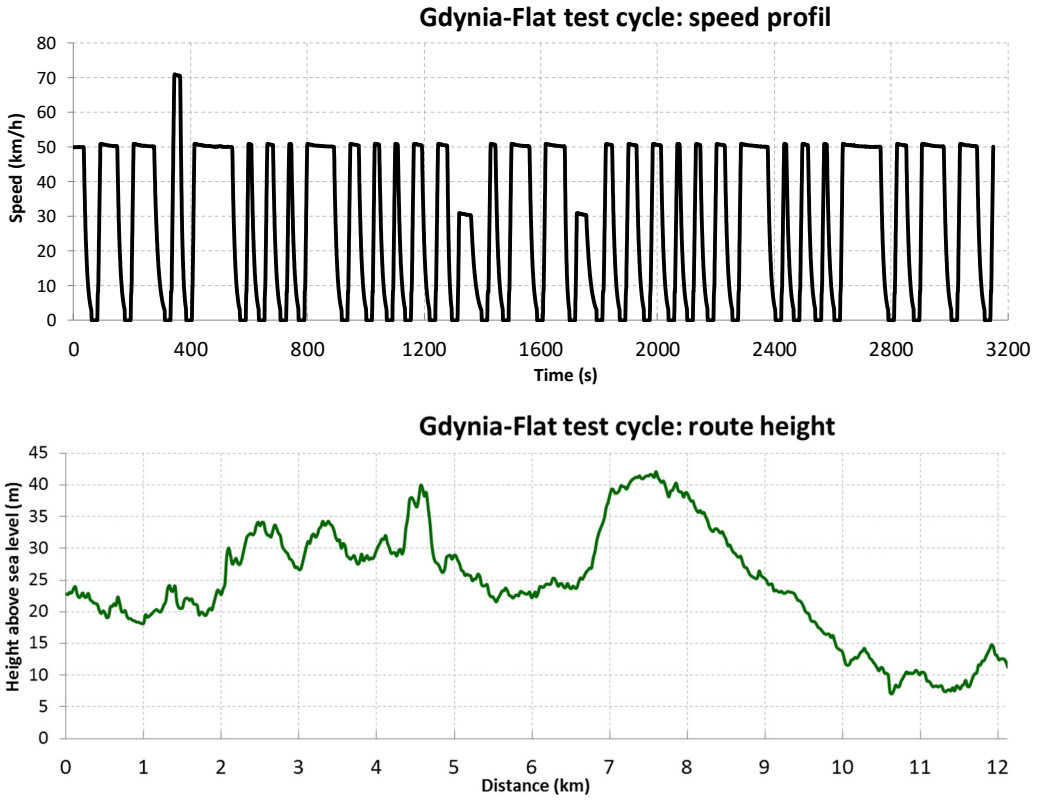

Figure 12. Gdynia-Flat route height and speed profiles.

Pursuant to the provisions of Subannexes 1 and 8 of Commission Regulation (EU) 2017/1151 [62], electric vehicles are classified as class 3b vehicles, or, if their maximum speed does not exceed 120 km/h, as class 3a. In line with the contents of Subannex 1, the energy consumption tests were carried out on the basis of the WLTC test cycles: Low3 phase (A1/7), Medium3-1 (A1/8) phase, High3-1 (A1/10) phase, Extra High3 (A1/12). The average vehicle speed in this cycle was 46.39 km/h, with a top speed of 131.3 km/h; the duration of the test was 1800 s and the length of the test route was 23.19 km. According to Paragraph 9 of Subannex 1, when the maximum speed of the vehicle is lower than the maximum speed of the cycle, speed modifications are to be applied [62].

The Gdynia-Flat test route was developed on the basis of real road conditions, and is characterized by variable speed with small changes in the slope of the terrain. The duration of the route was approx. 3200 s, the average speed of the vehicle was 27.19 km/h, the maximum speed was 70 km/h and the distance was approx. 25.4 km.

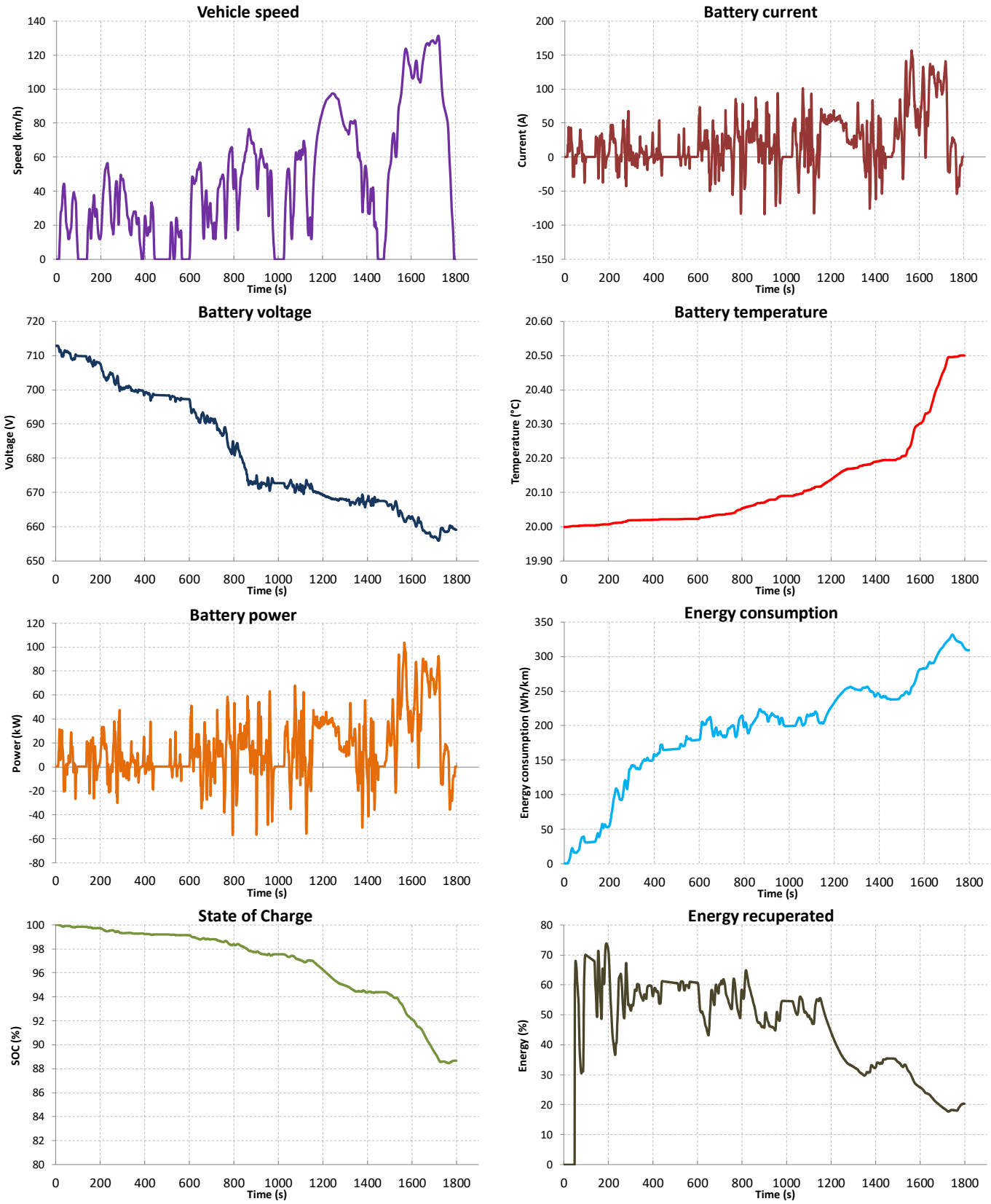

Figure 13. WLTC 3b-results of simulation tests for the 4 × 2 drive system.

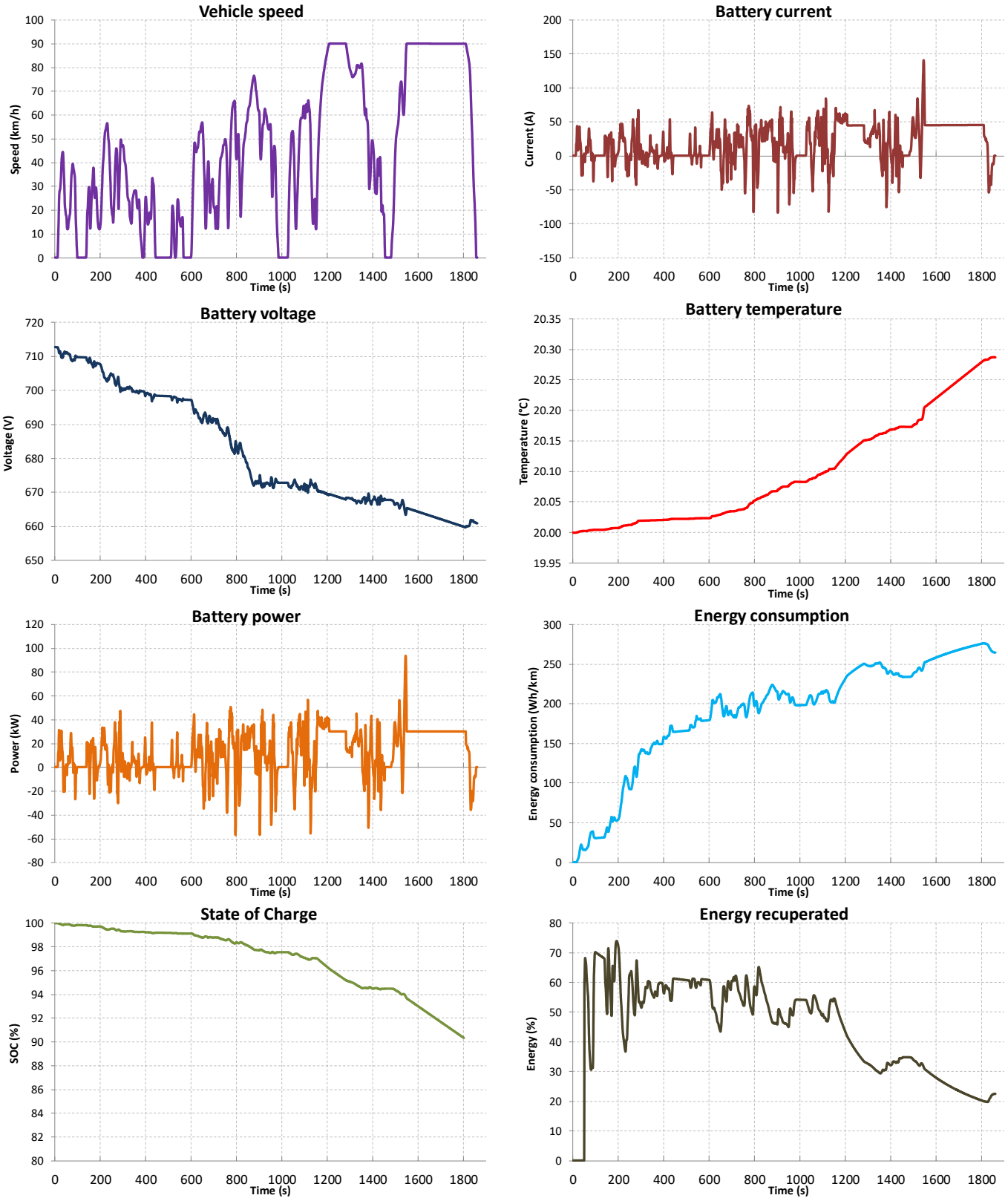

Figure 14. WLTC 3a-90-results of simulation tests for the 4 × 2 drive system.

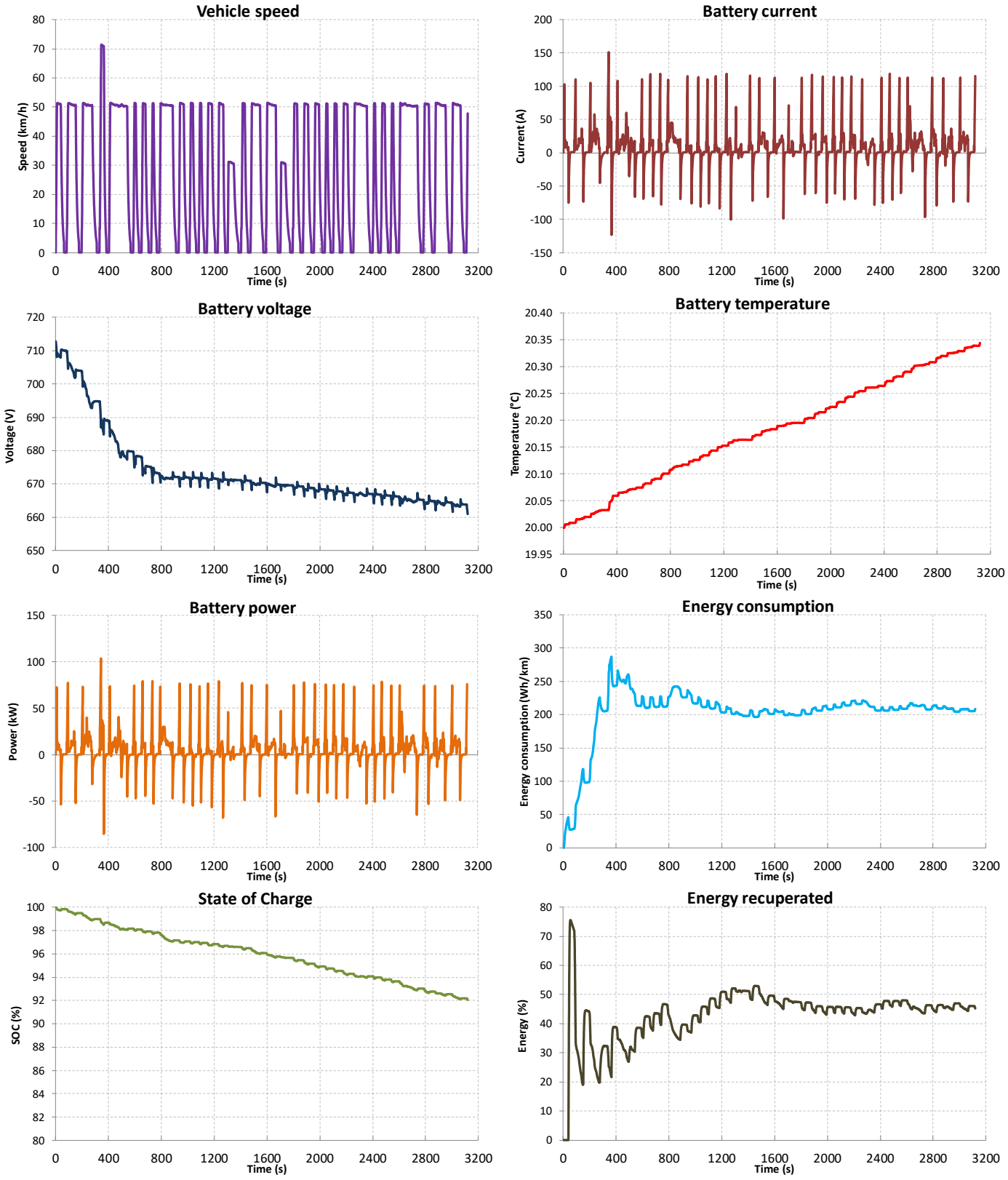

Figure 15. Results of simulation tests of the 4 × 2 drive system on the Gdynia-Flat route.

3.3. Tests of Energy Consumption by an Electric 4 × 4 Drive System

The test was carried out on the drive system in a 4 × 4 configuration with four motors located in the wheels, for which the developed mathematical model is presented in Section 2.1. The electric drive system consisted of four DWH-200 electric motors, capable of providing a maximum power exceeding 80 kW and a torque exceeding 1000 Nm. The motors were powered by STS-203 inverters, which made it possible to control drives with a power of 80 kW with a supply voltage from 12 to 850 VDC. The tests were carried out on the basis of the WLTC 3b, WLTC 3a-90 test cycles and the Gdynia-Flat test cycle. The results of the conducted research are presented in Figures 16–18.

Table 2 shows the energy consumption values depending on the drive system and the test route.

Table 2. Comparison of the energy consumption of electric drive systems in 4 × 2 and 4 × 4 configurations for different test cycles.

Test Cycle	Unit	4 × 2	4 × 4
WLTC 3b	Energy consumption (Wh/km)	308.8	289.4
	Range (km)	205.2	218.9
	Energy recuperated (%)	20.4	22.5
WLTC 3a-90	Energy consumption (Wh/km)	264.4	249.0
	Range (km)	239.6	254.5
	Energy recuperated (%)	22.5	24.5
Gdynia-Flat	Energy consumption (Wh/km)	208.3	187.1
	Range (km)	304.1	338.7
	Energy recuperated (%)	45.3	50.3

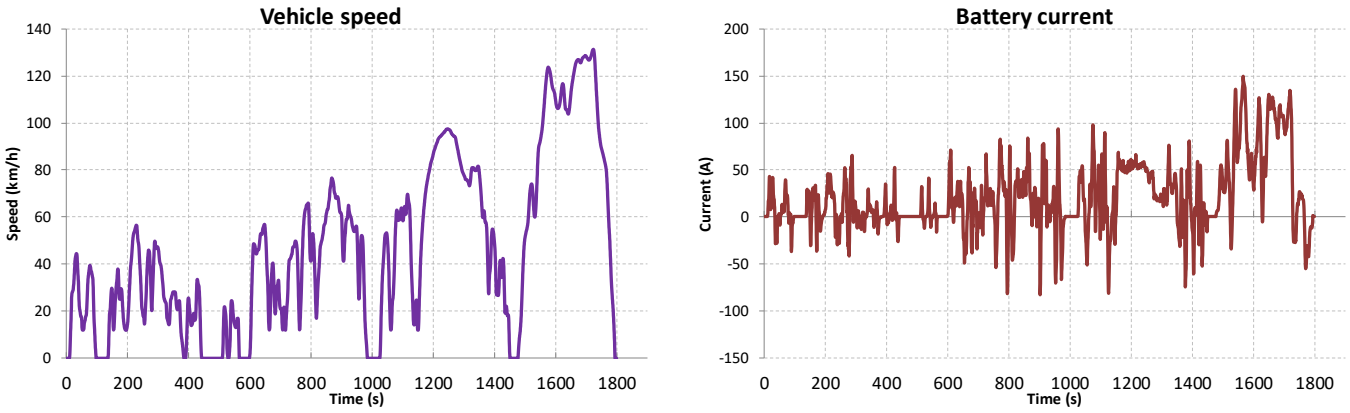

Figure 16. *Cont.*

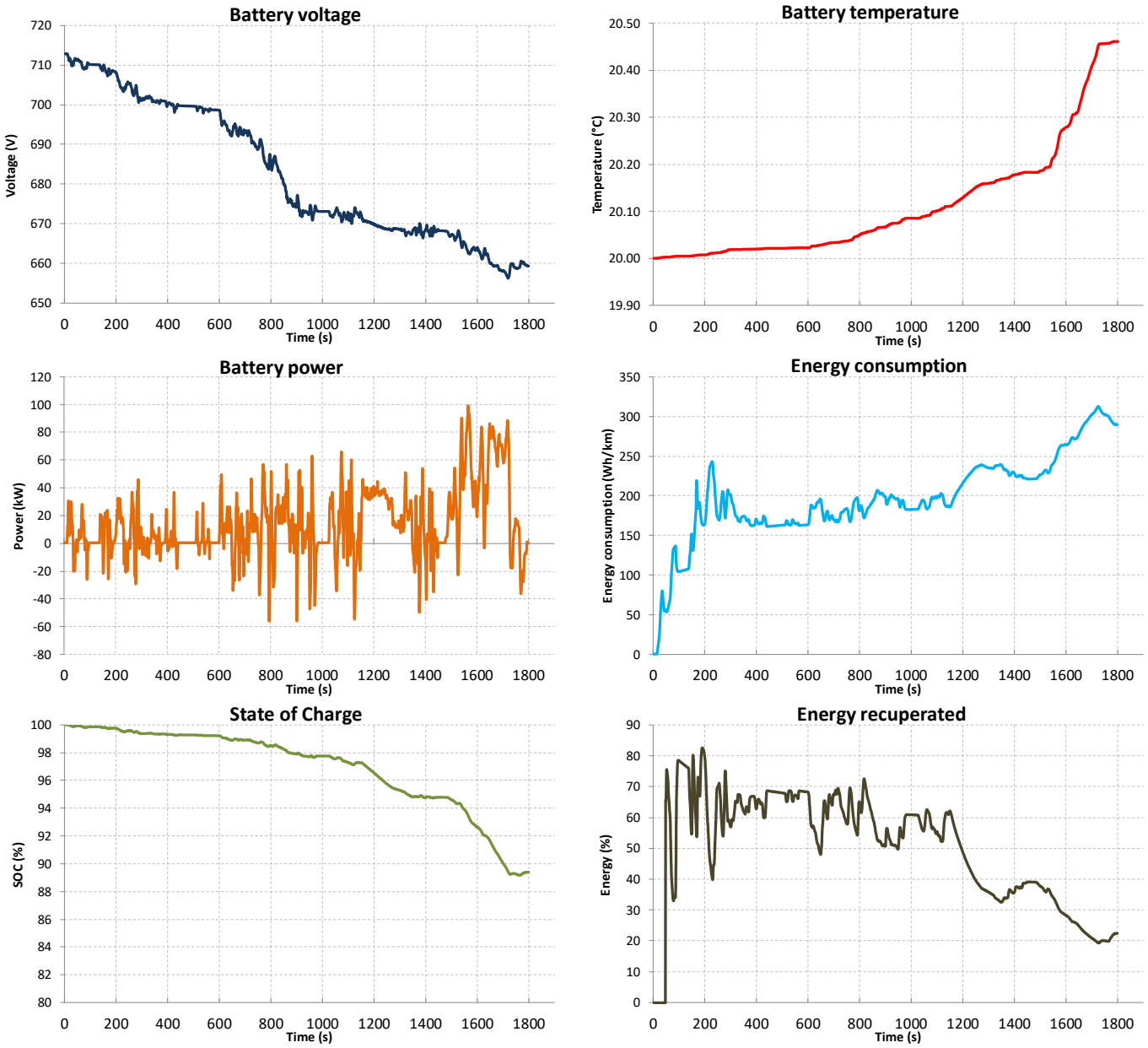

Figure 16. WLTC 3b-results of simulation tests for the 4 × 4 drive system.

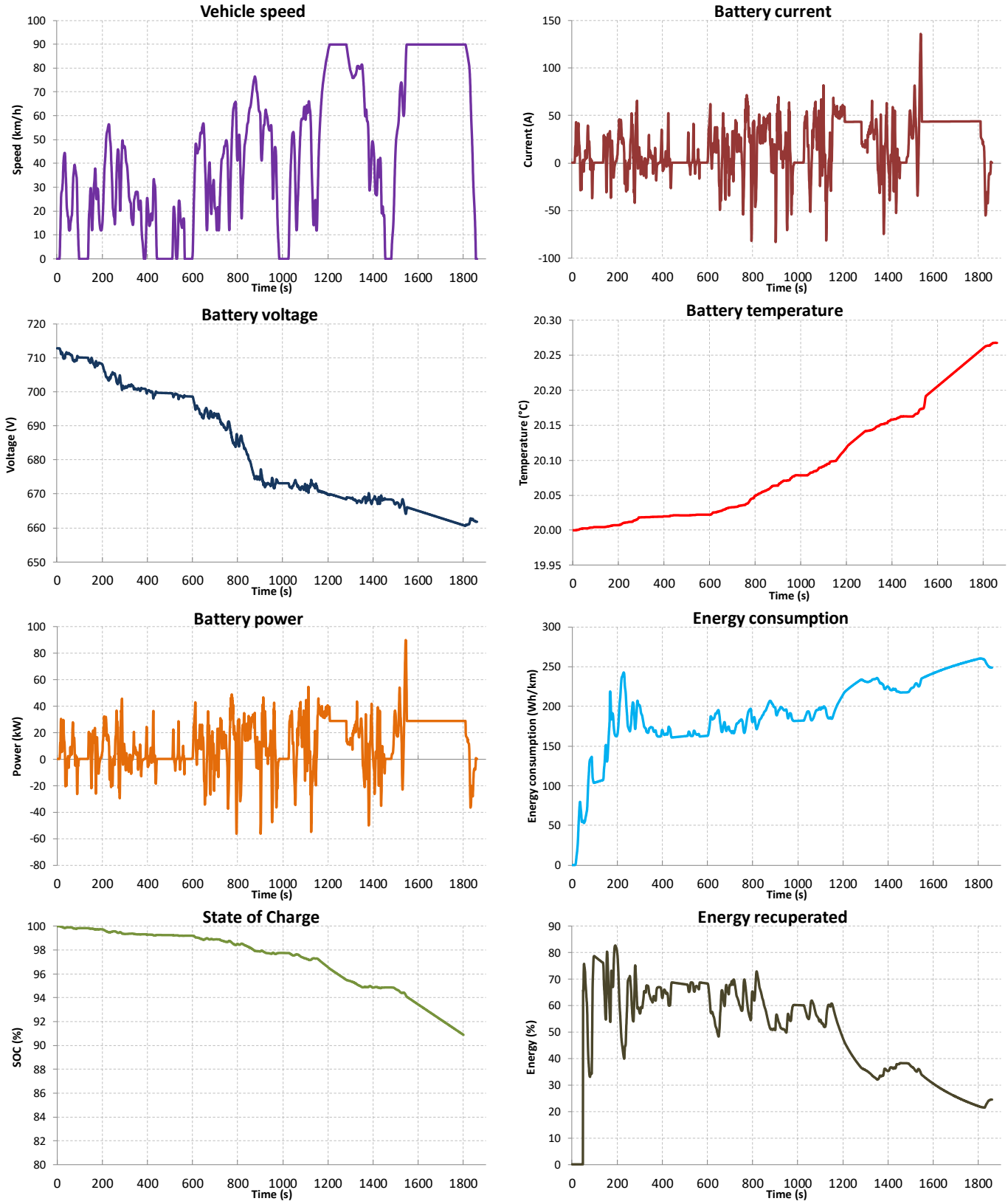

Figure 17. WLTC 3a-90-results of simulation tests for the 4 × 4 drive system.

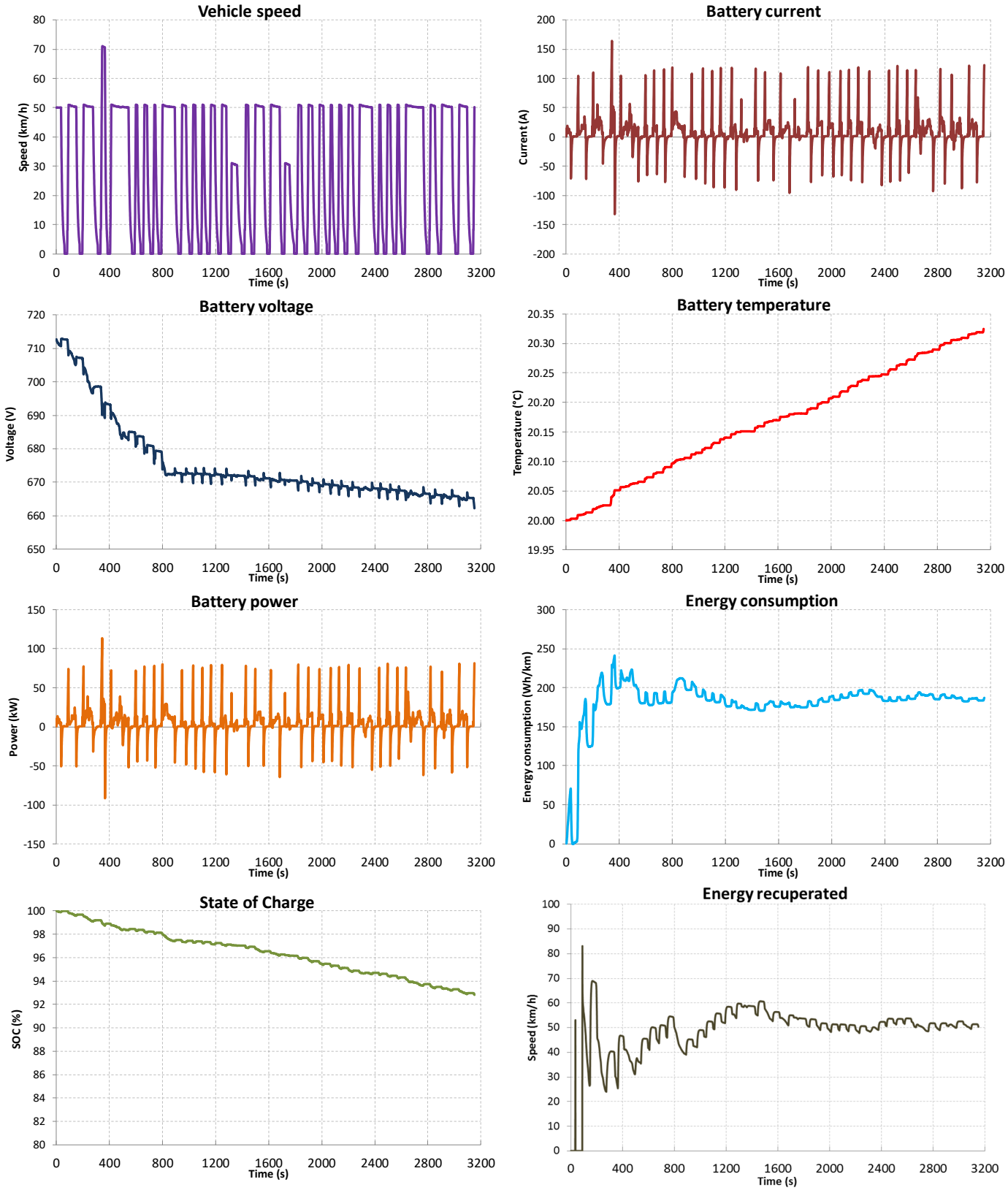

Figure 18. Results of simulation tests of the 4 × 4 drive system on the Gdynia-Flat route.

4. Discussion

4.1. Analysis of the Test Results of the Electric Drive Unit

The use of the concept of an electric drive unit installed in a vehicle wheel, in addition to the benefits of direct transmission of torque to the vehicle wheels, may have some negative effects in the form of increasing the unsprung mass of the vehicle. The unsprung mass consists of all movable suspension elements absorbing vibrations between the vehicle body and the ground on which it is moving (rims, tires, steering knuckles, rocker arms, hubs, driveshafts, brake calipers with pads and discs, steering rods, springs and shock absorbers). The sprung mass is the vehicle body with all its contents. Increasing the unsprung mass may adversely affect the comfort of traveling with the vehicle, as well as the strength of the suspension system structure to which the electric integrated drive module is mounted, i.e., the so-called motor in a wheel. The conducted research was aimed at verifying the influence of changes in the vehicle weight and the drive system components on the strength of the suspension components, as well as on the rolling resistance. The purpose of the research on the integrated suspension drive module was to verify the strength of the suspension system and the structure of the DWH-200 motor mounted in the wheel. The bench tests, conducted in laboratory conditions similar to real ones, were aimed at testing the suspension module with an integrated drive system with regard to the dynamics of work, traction properties and influence on steering. Track rollers were used for the tests, for which parameters could be set during acceleration and braking.

The main purpose of the present research was to determine whether the adopted/developed drive module suspension and the drive module itself would be able to meet the requirements of the standard related to carrying out strength and vibration tests ISO16750-3, Test IX "Commercial vehicles. Unsprung mass". The purpose of the IX test of the ISO16750-3 standard (4.1.2.9.1) is to verify the tested devices for malfunction and cracks due to vibrations. The test (4.1.2.9.2) was conducted based on the guidelines given in Table 15 of ISO16750-3. Depending on the rotational speed of a given roller, sinusoidal vibrations were obtained in accordance with the values presented in Table 15 of ISO16750-3 for the maximum values of the amplitude of accelerations on the wheels and wheel suspension, as well as the respective frequencies. The conducted research showed the correctness of the adopted design of the integrated drive module. During the tests, no damage or failures were observed, despite the fact that overloads of over 21G (21.23G; 208.24 m/s^2) occurred.

The conducted tests showed that the increase of unsprung mass by 71 kg (unsprung mass of a classic drive system: 79 kg; unsprung mass of the system with an electric drive module: 150 kg) did not negatively affect the work and strength of the entire suspension system. The increase of the unsprung mass did not have a significant influence on the increase of accelerations occurring either in the suspension elements of the vehicle or in the electric drive module. Increasing the unsprung mass reduced the acceleration of the wheel in the axis perpendicular to the ground (approx. −30%) and, at the same time, slightly increased the forces occurring in the suspension elements (approx. +6%). Thus, installing electric motors in eLCV wheels that are neither high speed nor sport driving can increase comfort for travelers.

4.2. Analysis of the Results of eLCV Tests with a 4 × 2 Drive System

The conducted research was aimed at verifying the influence of changes in vehicle weight and the configuration of the drive system elements on the value of the rolling resistance and, consequently, vehicle range. It is difficult to determine specific values for vehicle range and energy consumption, due to the fact that, in addition to aerodynamic drag, these parameters are influenced by a number of design, configuration and operational factors. The basic factors influencing the determination of the range and energy consumption parameters include: the configuration of the drive system, the parameters of the drive system (e.g., the level of regenerative braking, the drive control mode: Normal, Eco, Sport, Safe, algorithms which control the electric motor, driving style, tire pressure, energy consumption by on-board equipment, the efficiency of the cooling system of the

electric drive components, ambient temperature, vehicle loading level, the adopted test route, and even the level of window opening during operation.

During the tests for the WLTC 3b test track, the energy consumption of the vehicle was 308.8 Wh/km. With the introduction of a speed limit of 90 km/h (WLTC 3a-90), energy consumption was reduced to 264.4 Wh/km. The research carried out on the basis of the actual profile of the Gdynia-Flat route, characterized by maintaining the speed at a level not exceeding 70 km/h with the occurrence of small hills, resulted in a decrease in energy consumption to 208.3 Wh/km.

Energy consumption tests were carried out on the basis of Commission Regulation (EU) 2017/1151 [62], which provides for the possibility of modifying the speed during the test cycle. In practice, it is difficult to find test results based on the WLTC 3b test cycle. Examples of parameters provided by manufacturers showing energy consumption and the maximum speed of the vehicle during tests are as follows: Renault Master ZE 220 Wh/km, 100 km/h; Peugeot e-Boxer 250 Wh/km, 89 km/h; Citroen e-Relay 250 Wh/km, 89 km/h; Volkswagen e-Crafter 260 Wh/km, 90 km/h; Maxus e 280 Wh/km, 121 km/h; Fiat Ducato electric 280 Wh/km, 100 km/h; Mercedes e-Sprinter 345 Wh/km, 100 km/h. The obtained results for the 4 × 2 drive system, i.e., 308.8 Wh/km at 123 km/h and 264.4 Wh/km at 90 km/h, should therefore be considered satisfactory.

4.3. Analysis of the Results of eLCV Tests with a 4 × 4 Drive System

Adopting an electric drive in the wheel enables the chain torque transmission through the gears to be relimited. As a result, it is possible to obtain a greater range of the vehicle in relation to the classic drive, in which the torque is transmitted via gears or a bridge to the vehicle wheels. This is confirmed by the results of the obtained research. The 4 × 4 vehicle during the WLTC 3b test route achieved energy consumption of 289.4 Wh/km (6.3% less compared to the 4 × 2 configuration). For the WLTC 3a-90 road test with a speed limit of 90 km/h, the energy consumption was 249 Wh/km (5.8% less compared to the 4 × 2 configuration). During tests with the Gdynia-Flat test profile based on real road tests, the energy consumption was 187.1 Wh/km (10.2% less compared to the 4 × 2 configuration).

It should also be noted that a vehicle with a 4 × 4 drive system is characterized by a higher level of regenerative braking, i.e., by approx. 9% compared to a 4 × 2 drive system. Thanks to this property, it is possible to alleviate the working conditions of the energy storage by reducing consumption compared to a 4 × 2 drive system with the same traction conditions. This fact is of great importance, as it influences the extension of the service life of the most expensive element of the electric drive system, i.e., the energy storage module.

5. Conclusions

Tests of the drive modules of an eLCV (electric Light Commercial Vehicle) vehicle showed that an increase in unsprung mass from 79.41 kg to 150.63 kg did not adversely affect the operation and durability of the entire suspension. The increase in unsprung mass did not have a significant effect on the increase of forces acting on the pins and bolts securing the suspension to the body.

Increasing the unsprung mass resulted in a reduction in the acceleration of the wheel in the plane perpendicular to the ground, which may have a positive effect on passenger comfort.

The installation of electric drive motors in the wheels of the vehicle increases the loads occurring during operation in the tires and rims of the vehicle. When selecting rims and tires for the drive system with electric motors mounted in the wheels, one should consider using elements with increased load indexes.

Tire pressure has a significant impact on driving comfort and rolling resistance. If the tire pressure is too low (1 bar), the rolling resistance value can increase by more than 20% in relation to the nominal value (2.5 bar). An increase in the tire pressure to 5.5 bar has little effect on the increase in the rolling resistance value (up to 3.5%).

The conducted research confirmed that the use of an electric drive system with motors mounted in the wheels contributes to the reduction of losses in the drive system, as compared to a classic system with a single motor and transmission. The conducted tests showed that the system with the drive in the 4 × 4 configuration can achieve a greater range in the WLTC test by up to about 6%, compared to the system in the 4 × 2 configuration on the same test route. It should be taken into account that, unfortunately, the investment cost of a drive system with four drive modules may be three times higher than that of a system with one central engine. A slight consolation may be the fact that the drive system in 4 × 4 configuration, thanks to its greater efficiency compared to the 4 × 2 system, reduces the load on the energy storage system, thereby extending its life-cycle. In addition, the 4 × 4 drive system is more reliable than the 4 × 2 system.

Thanks to the use of a wet brake built into the motor in the wheel, it is possible to completely eliminate the release of the dust into the environment which occurs with classic brake systems with drums or discs. At the same time, the 4 × 4 system provides greater reliability for the vehicle, as well as better traction.

Author Contributions: Conceptualization, P.S. and A.Ł.; computations, P.S. and A.Ł.; methodology, P.S. and A.Ł.; experimental verification, P.S. and A.Ł.; writing text of the article, P.S. and A.Ł.; review and editing, P.S. and A.Ł.; visualization, P.S. and A.Ł.; supervision, P.S. and A.Ł. All authors have read and agreed to the published version of the manuscript.

Funding: The research presented in this publication has been supported by founding from the project financed by National Centre for Research and Development named "Development of an innovative drive for mobile platforms", project no. POIR.01.01.01-00-0075/17, total value 19,133,242,26 PLN.

Institutional Review Board Statement: Not applicable.

Informed Consent Statement: Not applicable.

Data Availability Statement: Not applicable.

Conflicts of Interest: The authors declare no conflict of interest.

Abbreviations

The following abbreviations are used in this manuscript:

eLCV	electric Light Commercial Vehicle
4 × 2	Drive system with one central motor and inverter powered from the energy storage
4 × 4	Drive system with four motors in the vehicle wheels controlled by inverters powered from the energy storage (battery pack)
NEDC	New European Driving Cycle
WLTC	Worldwide Harmonized Light Vehicles Test Cycle
BATT	Battery pack, energy storage
PE	Power Electronics (Inverter)
EM	Electric Motor
T	Transmission
DWH-200	(Drive WHeel) Electric motor integrated with the wheel hub, developed and produced by WB GROUP, Zakład Automatyki i Urządzeń Pomiarowych AREX Sp. z o.o., Gdynia, Poland
WHB-200	Wet (dust-free) brake designed to be integrated with the DWH-200 engine. All developed and produced by WB GROUP, Zakład Automatyki i Urządzeń Pomiarowych AREX Sp. z o.o., Gdynia, Poland
DCE-200	(Drive CEntral) Electric motor, developed and produced by WB GROUP, Zakład Automatyki i Urządzeń Pomiarowych AREX Sp. z o.o., Gdynia, Poland

STS-202, STS-202	Inverters for controlling the operation of synchronous motors, developed and manufactured by WB GROUP, Zakład Automatyki i Urządzeń Pomiarowych AREX Sp. z o.o., Gdynia, Poland
BAT-200	Energy storage consisting of electrochemical cells of LiFePO4 type, developed and produced by WB GROUP, Zakład Automatyki i Urządzeń Pomiarowych AREX Sp. z o.o., Gdynia, Poland

References

1. Chai, F.; Bi, Y.; Chen, L. A Comparison between Axial and Radial Flux Permanent Magnet In-Wheel Motors for Electric Vehicle. In Proceedings of the 2020 International Conference on Electrical Machines (ICEM), Gothenburg, Sweden, 23–26 August 2020; IEEE: Piscataway, NJ, USA, 2020; pp. 1685–1690, ISBN 978-1-7281-9945-0.
2. Chawrasia, S.K.; Kumar Chanda, C.; Banerjee, S. Design and Analysis of In-Wheel Motor for an Electric Vehicle. In Proceedings of the CALCON 2020, 2020 IEEE Calcutta Conference, Kolkata, India, 28–29 February 2020; Ray, S., Kundu, A., Na, T., Eds.; IEEE: Piscataway, NJ, USA, 2020; pp. 351–355, ISBN 978-1-7281-4283-8.
3. Kazak, A.N.; Filippov, D.M. Development of In-wheel Motor for Vehicles. In Proceedings of the 2019 IEEE Conference of Russian Young Researchers in Electrical and Electronic Engineering (EIConRus), Saint Petersburg, Russia, 28–31 January 2019; Shaposhnikov, S.O., Ed.; IEEE: Piscataway, NJ, USA, 2019; pp. 1406–1408, ISBN 978-1-7281-0339-6.
4. Guo, X.; Chen, Y.; Li, H. Research on Steering Stability Control of Electric Vehicle Driven by Dual In-Wheel Motor. In Proceedings of the 2020 10th Institute of Electrical and Electronics Engineers International Conference on Cyber Technology in Automation, Control, and Intelligent Systems (CYBER), Xi'an, China, 10–13 October 2020; IEEE: Piscataway, NJ, USA, 2020; pp. 394–399, ISBN 978-1-7281-9010-5.
5. Tseng, Y.-H.; Yang, Y.-P. An Energy Saving Strategy of Torque and Battery Distribution for an Electric Vehicle Driven by Multiple Traction Motors. In Proceedings of the 2019 Electric Vehicles International Conference (EV), Bucharest, Romania, 3–4 October 2019; IEEE: Piscataway, NJ, USA, 2019; pp. 1–6, ISBN 978-1-7281-0791-2.
6. Liang, P.; Chai, F.; Shen, K.; Liu, W. Thermal design and optimization of a water-cooling permanent magnet synchronous in-wheel motor. In Proceedings of the 2019 22nd International Conference on Electrical Machines and Systems (ICEMS), Harbin, China, 11–14 August 2019; IEEE: Piscataway, NJ, USA, 2019; pp. 1–6, ISBN 978-1-7281-3398-0.
7. Wicher, J.; Wieckowski, D. Influence of Vibrations of the Child Seat on the Comfort of Child's Ride in a Car. *Maint. Reliab.* **2010**, *2010*, 102–110.
8. Wang, G.; Chen, X.; Xing, Y.; Liu, H.; Tian, D. Optimal design of an interior permanent magnet in-wheel motor for electric off-road vehicles. In Proceedings of the 2018 IEEE International Conference on Electrical Systems for Aircraft, Railway, Ship Propulsion and Road Vehicles & International Transportation Electrification Conference (ESARS-ITEC), Nottingham, UK, 7–9 November 2018; pp. 1–5, ISBN 978-1-5386-4192-7.
9. Fu, X.; Yuan, Y.; Liu, D.; Zhang, Q.; Pei, J. Fault Tolerance Control of Four In-wheel Motors Driven Vehicles Based on Limping Dynamic Performance. In Proceedings of the 2020 3rd International Conference on Electron Device and Mechanical Engineering (ICEDME), Suzhou, China, 1–3 May 2020; Conference Publishing Services, IEEE Computer Society: Los Alamitos, CA, USA, 2020; pp. 352–359, ISBN 978-1-7281-8145-5.
10. Nah, J.; Yim, S. Vehicle Stability Control with Four-Wheel Independent Braking, Drive and Steering on In-Wheel Motor-Driven. *Electr. Vehicles. Electron.* **2020**, *9*, 1934. [CrossRef]
11. Park, G.; Han, K.; Nam, K.; Kim, H.; Choi, S.B. Torque Vectoring Algorithm of Electronic-Four-Wheel Drive Vehicles for Enhancement of Cornering Performance. *IEEE Trans. Veh. Technol.* **2020**, *69*, 3668–3679. [CrossRef]
12. Lucchini, A.; Formentin, S.; Corno, M.; Piga, D.; Savaresi, S.M. Torque Vectoring for High-Performance Electric Vehicles: An Efficient MPC Calibration. *IEEE Control Syst. Lett.* **2020**, *4*, 725–730. [CrossRef]
13. Lee, K.; Lee, M. Fault-Tolerant Stability Control for Independent Four-Wheel Drive Electric Vehicle Under Actuator Fault Conditions. *IEEE Access* **2020**, *8*, 91368–91378. [CrossRef]
14. Jin, X.; Wang, J.; Sun, S.; Li, S.; Yang, J.; Yan, Z. Design of Constrained Robust Controller for Active Suspension of In-Wheel-Drive Electric Vehicles. *Mathematics* **2021**, *9*, 249. [CrossRef]
15. Wu, H.; Zheng, L.; Li, Y.; Zhang, Z.; Yu, Y. Robust Control for Active Suspension of Hub-Driven Electric Vehicles Subject to in-Wheel Motor Magnetic Force Oscillation. *Appl. Sci.* **2020**, *10*, 3929. [CrossRef]
16. Chen, C.; Cheng, Y.; Meng, F. Optimum Design of a Novel In-Wheel Suspension of the Electric Wheel. In Proceedings of the 2019 IEEE 3rd International Conference on Green Energy and Applications (ICGEA), Taiyuan, China, 16–18 March 2019; IEEE: Piscataway, NJ, USA, 2019; pp. 106–110, ISBN 978-1-7281-1383-8.
17. Tian, M.; Gao, B. Dynamics analysis of a novel in-wheel powertrain system combined with dynamic vibration absorber. *Mech. Mach. Theory* **2021**, *156*, 104148. [CrossRef]
18. Liu, M.; Gu, F.; Zhang, Y. Ride Comfort Optimization of In-Wheel-Motor Electric Vehicles with In-Wheel Vibration Absorbers. *Energies* **2017**, *10*, 1647. [CrossRef]
19. Tian, J.; Ding, J.; Zhang, C.; Luo, S. Four-Wheel Differential Steering Control of IWM Driven EVs. *IEEE Access* **2020**, *8*, 152963–152974. [CrossRef]

20. Dornier, P. European Parliament Votes to End Dirty Diesel's Licence to Pollute. Transport & Environment [Online]. 16 September 2020. Available online: https://www.transportenvironment.org/press/european-parliament-votes-end-dirty-diesel%E2%80%99s-licence-pollute (accessed on 10 November 2020).
21. *Air Quality in Europe: 2019 Report*; Publications Office of the European Union: Luxembourg, 2019; ISBN 9789294800886.
22. Przybyłowski, A. Sustainable Transport Planning & Development in the EU at the Example of the Polish Coastal Region Pomorskie. *Transp. Syst. Process. Mar. Navig. Saf. Sea Transp.* **2011**, *2011*, 101–109.
23. Neumann, T. The Impact of Carsharing on Transport in the City. Case Study of Tri-City in Poland. *Sustainability* **2021**, *13*, 688. [CrossRef]
24. Air Pollution—European Environment. AgencyAir Pollution is the Biggest Environmental Health Risk in Europe. Available online: https://www.eea.europa.eu/themes/air (accessed on 10 November 2020).
25. Foundation, T.R. Which Countries Have Banned Petrol and Diesel Cars? Available online: https://news.trust.org/item/20201118095737-8h1uh (accessed on 15 February 2021).
26. REGULATION (EU) 2019/2144 of the European Parliament and of the Council. Available online: https://eur-lex.europa.eu/eli/reg/2019/2144/oj (accessed on 15 February 2021).
27. Gibson, D. Best Electric Vans 2020. Auto Express [Online]. Available online: https://www.autoexpress.co.uk/vans/105891/best-electric-vans-2020 (accessed on 12 November 2020).
28. de Pinto, S.; Camocardi, P.; Chatzikomis, C.; Sorniotti, A.; Bottiglione, F.; Mantriota, G.; Perlo, P. On the Comparison of 2- and 4-Wheel-Drive Electric Vehicle Layouts with Central Motors and Single- and 2-Speed Transmission Systems. *Energies* **2020**, *13*, 3328. [CrossRef]
29. VN5 | Electric Commercial Vehicle | New Electric Van | Hybrid Van. Available online: https://www.levc.com/vn5-electric-lcv-van/ (accessed on 23 February 2021).
30. Hoang, N.-T.; Yan, H.-S. On the Design of In-Wheel-Hub Motor Transmission Systems with Six-Link Mechanisms for Electric Vehicles. *Energies* **2018**, *11*, 2920. [CrossRef]
31. Tajima, D.; Shimizu, O.; Fujimoto, H. High-Efficiency Operation of Wireless In-Wheel Motor at Low Load Using Intermittent Synchronous Rectification with Improved Transient Stability. In Proceedings of the IECON 2019—45th Annual Conference of the IEEE Industrial Electronics Society, Lisbon, Portugal, 14–17 October 2019; IEEE: Piscataway, NJ, USA, 2019; pp. 1089–1094, ISBN 978-1-7281-4878-6.
32. Fujimoto, H.; Shimizu, O.; Nagai, S.; Fujita, T.; Gunji, D.; Ohmori, Y. Development of Wireless In-wheel Motors for Dynamic Charging: From 2nd to 3rd generation. In Proceedings of the 2020 IEEE PELS Workshop on Emerging Technologies: Wireless Power Transfer (WoW), Seoul, Korea, 15–19 November 2020; IEEE: Piscataway, NJ, USA, 2020; pp. 56–61, ISBN 978-1-7281-3746-9.
33. Gao, P.; Gu, Y.; Wang, X. The Design of a Permanent Magnet In-Wheel Motor with Dual-Stator and Dual-Field-Excitation Used in Electric Vehicles. *Energies* **2018**, *11*, 424. [CrossRef]
34. Elaphe. Solutions—Elaphe. Available online: http://in-wheel.com/en/ (accessed on 22 February 2021).
35. ZIEHL-ABEGG USA—In-Wheel Hub Motors. Available online: https://global.ziehl-abegg.com/us/en/product-range/automotive/in-wheel-hub-motors/ (accessed on 22 February 2021).
36. Motors, G. In-Wheel Motors and Electric Drive Solutions. Available online: https://www.gemmotors.si/ (accessed on 22 February 2021).
37. Protean. Technology—Protean. Available online: https://www.proteanelectric.com/technology/#overview (accessed on 22 February 2021).
38. Dukalski, P.; Krok, R. Selected Aspects of Decreasing Weight of Motor Dedicated to Wheel Hub Assembly by Increasing Number of Magnetic Poles. *Energies* **2021**, *14*, 917. [CrossRef]
39. Dukalski, P.; Będkowski, B.; Parczewski, K.; Wnęk, H.; Urbaś, A.; Augustynek, K. Dynamics of the vehicle rear suspension system with electric motors mountedin wheels. *Maint. Reliab.* **2018**, *21*, 125–136. [CrossRef]
40. Bedkowski, B.; Dukalski, P.; Jarek, T.; Wolnik, T. Numerical model for thermal calculation analysis of the wheel hub motor for electric car verified by laboratory tests. *IOP Conf. Ser. Mater. Sci. Eng.* **2020**, *710*, 012018. [CrossRef]
41. Di Gerlando, A.; Foglia, G.; Ricca, C. Analytical Design of a High Torque Density In-Wheel YASA AFPM Motor. In Proceedings of the 2020 International Conference on Electrical Machines (ICEM), Gothenburg, Sweden, 23–26 August 2020; IEEE: Piscataway, NJ, USA, 2020; pp. 402–408, ISBN 978-1-7281-9945-0.
42. Abramowicz-Gerigk, T.; Burciu, Z.; Hapke, L. Innovative Project of Propellers and Thrusters Jet Loads during Ship Berthing Monitoring System. *TransNav* **2019**, *13*, 861–865. [CrossRef]
43. EMRAX. EMRAX | Axial Flux E-Motors | Lightweight | Powerful—EMRAX. Available online: https://emrax.com/ (accessed on 22 February 2021).
44. Vansompel, H.; Leijnen, P.; Sergeant, P. Multiphysics Analysis of a Stator Construction Method in Yokeless and Segmented Armature Axial Flux PM Machines. *IEEE Trans. Energy Convers.* **2019**, *34*, 139–146. [CrossRef]
45. Zhang, X.; Zhang, W.; Yu, F. Optimal Design of a Hybrid Excitation Axial Flux-Switching In-Wheel Motor. In Proceedings of the 2018 Asia Pacific Magnetic Recording Conference (APMRC), Shanghai, China, 15–17 November 2018; IEEE: Piscataway, NJ, USA, 2018; pp. 1–2, ISBN 978-1-5386-8378-1.
46. Winterborne, D.; Stannard, N.; Sjoberg, L.; Atkinson, G. An Air-Cooled YASA Motor for in-Wheel Electric Vehicle Applications. *IEEE Trans. Ind. Appl.* **2020**, *56*, 6448–6455. [CrossRef]

47. Chen, Q.; Liang, D.; Jia, S.; Ze, Q.; Liu, Y. Analysis of Winding MMF and Loss for Axial Flux PMSM With FSCW Layout and YASA Topology. *IEEE Trans. Ind. Appl.* **2020**, *56*, 2622–2635. [CrossRef]
48. Mohamed-Seghir, M.; Krama, A.; Refaat, S.S.; Trabelsi, M.; Abu-Rub, H. Artificial Intelligence-Based Weighting Factor Autotuning for Model Predictive Control of Grid-Tied Packed U-Cell Inverter. *Energies* **2020**, *13*, 3107. [CrossRef]
49. Anaya-Martinez, M.; Lozoya-Santos, J.-d.-J.; Félix-Herrán, L.C.; Tudon-Martinez, J.-C.; Ramirez-Mendoza, R.-A.; Morales-Menendez, R. Control of Automotive Semi-Active MR Suspensions for In-Wheel Electric Vehicles. *Appl. Sci.* **2020**, *10*, 4522. [CrossRef]
50. Sun, W.; Li, Q.; Sun, L.; Li, L. Development and Investigation of Novel Axial-Field Dual-Rotor Segmented Switched Reluctance Machine. *IEEE Trans. Transp. Electrif.* **2020**. [CrossRef]
51. Keskin Arabul, F.; Senol, I.; Oner, Y. Performance Analysis of Axial-Flux Induction Motor with Skewed Rotor. *Energies* **2020**, *13*, 4991. [CrossRef]
52. Evans Electric. Evans Electric. Available online: https://www.evans-electric.com.au/ (accessed on 23 February 2021).
53. Wiśniewski, G.; Buda, T.; Kref, O. Application of electric drive system for electric delivery cars—Part I. *Electrotech. News* **2020**, *1*, 5–13. [CrossRef]
54. Wiśniewski, G.; Buda, T.; Kref, O. Application of electric drive system for electric delivery cars—Part II. *Electrotech. News* **2020**, *1*, 5–12. [CrossRef]
55. Dana TM4. Commercial Vehicles | Dana TM4. Available online: https://www.danatm4.com/vehicle-applications/commercial-vehicles/ (accessed on 23 February 2021).
56. Schuetz, T. *Aerodynamics of Road Vehicles, 5th ed by Thomas Schuetz*; SAE International: Warrendale, PA, USA, 2016; ISBN 9780768079777.
57. Landa, H.C. *The Automotive Aerodynamics Handbook: Including Practical Problems Workbook*, 8th ed., rev. and enl; Film Instruction Company of America: Milwaukee, WI, USA, 1999; ISBN 0931974186.
58. The Engineering ToolBox. Rolling Resistance—Rolling Friction and Rolling Resistance. Available online: https://www.engineeringtoolbox.com/rolling-friction-resistance-d_1303.html (accessed on 15 September 2021).
59. Heisler, H. *Advanced Vehicle Technology*, 2nd ed.; Butterworth-Heinemann: Oxford, UK, 2002; ISBN 9780080493442.
60. Emission Test Cycles: WLTC. Available online: https://dieselnet.com/standards/cycles/wltp.php (accessed on 18 September 2021).
61. Emission Test Cycles: ECE 15 + EUDC/NEDC. Available online: https://dieselnet.com/standards/cycles/ece_eudc.php (accessed on 18 September 2021).
62. Commission Regulation (EU) 2017/1151 of 1 June 2017 supplementing Regulation (EC) No 715/2007 of the European Parliament and of the Council on Type-Approval of Motor Vehicles With Respect to Emissions from Light Passenger and Commercial Vehicles (Euro 5 and Euro 6) and on Access to Vehicle Repair and Maintenance Information, Amending Directive 2007/46/EC of the European Parliament and of the Council, Commission Regulation (EC) No 692/2008 and Commission Regulation (EU) No 1230/2012 and Repealing Commission Regulation (EC) No 692/2008. Available online: https://eur-lex.europa.eu/legal-content/EN/TXT/?uri=CELEX%3A32017R1151 (accessed on 18 September 2021).